Automatica 131 (2021) 109743

Contents lists available at ScienceDirect

Automatica

journal homepage: www.elsevier.com/locate/automatica

Polynomial chaos-based $\mathcal{H}_2$ output-feedback control of systems with probabilistic parametric uncertainties☆

Yiming Wan [a,b,1], Dongying Erin Shen [c,1], Sergio Lucia [d], Rolf Findeisen [e], Richard D. Braatz [c,*]

[a] School of Artificial Intelligence and Automation, Huazhong University of Science and Technology, Wuhan 430074, China
[b] Key Laboratory of Image Processing and Intelligent Control, Ministry of Education China, China
[c] Massachusetts Institute of Technology, Cambridge, MA 02139, USA
[d] TU Dortmund University, 44227 Dortmund, Germany
[e] Laboratory for Systems Theory and Automatic Control, Otto-von-Guericke University Magdeburg, 39106 Magdeburg, Germany

ARTICLE INFO

Article history:
Received 24 February 2020
Received in revised form 21 February 2021
Accepted 9 May 2021
Available online 9 June 2021

Keywords:
Output-feedback
Robust control
Parametric uncertainties
Polynomial chaos
Stochastic systems

ABSTRACT

$\mathcal{H}_2$ static and dynamic output-feedback control problems are investigated for linear time-invariant uncertain systems. The goal is to minimize the averaged $\mathcal{H}_2$ performance in the presence of nonlinear dependence on time-invariant probabilistic parametric uncertainties. By applying the polynomial chaos theory, the control synthesis problem is solved using a high-dimensional expanded system which characterizes stochastic state uncertainty propagation. Compared to existing polynomial chaos-based control designs, the proposed approach addresses the simultaneous presence of parametric uncertainties and white noises. The effect of truncation errors due to using finite-degree polynomial chaos expansions is captured by time-varying norm-bounded uncertainties, and is explicitly taken into account by adopting a guaranteed cost control approach. This feature avoids the use of high-degree polynomial chaos expansions to alleviate the destabilizing effect of expansion truncation errors, thus significantly reducing computational complexity. Moreover, rigorous analysis clarifies the condition under which the stability of the high-dimensional expanded system implies the internal mean square stability of the original system under control. Using iterations between synthesis and post-analysis, a bisection algorithm is proposed to find the smallest bounding parameter on the effect of expansion truncation errors such that robust closed-loop stability is guaranteed. A numerical example is used to illustrate the effectiveness of the proposed approach.

© 2021 Elsevier Ltd. All rights reserved.

1. Introduction

The closed-loop stability and performance obtained by state- and output-feedback control systems can be sensitive to model uncertainties, which has motivated numerous studies on the synthesis of robust control insensitive to uncertainties, e.g., Ahn et al. (2018), Chang et al. (2015), Dong and Yang (2013), Lee et al. (2015), Petersen and Tempo (2014), Sadabadi and Peaucelle (2016), Salavati et al. (2019) and Rosa et al. (2018). The static or reduced-order dynamic output-feedback control synthesis problem for both nominal and uncertain systems is NP-hard, which implies that standard linear matrix inequalities (LMIs) and other convex optimization formulations do not exist (Sadabadi & Peaucelle, 2016).

The majority of the output-feedback and broader control literature adopts a worst-case design strategy to ensure stability and achieve a desired performance bound for all possible uncertainties. This worst-case approach tends to produce highly conservative performance because the worst-case scenario may have vanishingly low probability of occurrence. In addition, most worst-case approaches are limited to specific uncertainty structures, such as norm-bounded, affine, polytopic, and integral quadratic uncertainties (Petersen & Tempo, 2014). A general nonlinear uncertainty structure cannot be effectively addressed without introducing overbounds.

In contrast to a worst-case performance bound, the practical interest in the performance variation or dispersion across the

☆ This work is supported by the National Natural Science Foundation of China under Grant No. 61803163, and the DARPA, USA Make-It program under contract ARO W911NF-16-2-0023. The material in this paper was partially presented at the 20th IFAC World Congress of the International Federation of Automatic Control, July 9–14, 2017, Toulouse, France (Shen et al., 2017). This paper was recommended for publication in revised form by Associate Editor Oswaldo Luiz V. Costa under the direction of Editor Sophie Tarbouriech.

* Corresponding author.
E-mail addresses: ywan@hust.edu.cn (Y. Wan), dongying@mit.edu (D.E. Shen), sergio.lucia@tu-dortmund.de (S. Lucia), rolf.findeisen@ovgu.de (R. Findeisen), braatz@mit.edu (R.D. Braatz).

[1] Yiming Wan and Dongying E. Shen equally contributed to this work.

https://doi.org/10.1016/j.automatica.2021.109743
0005-1098/© 2021 Elsevier Ltd. All rights reserved.

uncertainty region has motivated recent research on probabilistic robustness (Petersen & Tempo, 2014). The design objectives then include second-moment stability (Hosoe et al., 2018), a probability-guaranteed performance bound (Tempo et al., 2013; Yin et al., 2018), or an optimal averaged performance (Boyarski & Shaked, 2005). In this line of research, literature like Hosoe et al. (2018) assume the uncertain parameters to be independent and identically distributed stochastic processes. This assumption allows arbitrarily fast parameter variations, which is not true in some applications. The randomized algorithm proposed in Tempo et al. (2013) can address general nonlinear dependence on uncertain parameters, but can be computationally demanding since a large number of samples is often needed.

The above observations have further led to robust control research that aims at addressing averaged performance in the presence of general nonlinear dependence on probabilistic time-invariant parametric uncertainties. Such an uncertainty description is commonly generated by parameter identification techniques, but is poorly suited for any existing robust control design methods mentioned above. This robust control problem is non-trivial because uncertainty propagation in such an uncertain system is no longer a Markov process when accounting for the time invariance of uncertain parameters (Paulson et al., 2015). As a computationally efficient non-sampling approach for quantifying uncertainty propagation, polynomial chaos (PC) theory builds the foundation of a recent promising solution to this problem (Kim et al., 2013). PC theory allows characterization of the evolution of probability distributions of the underlying stochastic system states by a high-dimensional expanded deterministic system describing the evolution dynamics of the polynomial chaos expansion (PCE) coefficients. Thus the control synthesis problem can be solved by using the PCE-transformed system. Up to now, the existing PCE-based control methods have been applied to stability analysis (Hover & Triantafyllou, 2006; Lucia et al., 2017), state-feedback control (Bhattacharya, 2019; Fisher & Bhattacharya, 2009; Hsu & Bhattacharya, 2017), optimal control (Bergner & Kirches, 2018; Lefebvre et al., 2020; Nandi & Singh, 2018; Paulson & Mesbah, 2019), and stochastic model predictive control (Dai et al., 2015; Paulson et al., 2015). Except for Konda et al. (2011), most of the published methods do not simultaneously consider time-invariant random parametric uncertainties and time-varying stochastic external disturbances, because applying PCE to compute the uncertainty propagation of time-varying stochastic disturbances involves infinite number of random variables as time goes to infinity. Moreover, due to truncation errors introduced by using finite-degree PCEs, stability and performance derived for the PCE-transformed system may not be automatically achieved by the original system (Lucia et al., 2017). Although increasing the PCE degree can alleviate the effect of PCE truncation errors, it may result in significant increase in computational complexity as the state dimension of the PCE-transformed system factorially grows with the PCE degree.

In this article, PCE-based $\mathcal{H}_2$ static and dynamic output-feedback controls are investigated. Both nonlinear dependence on probabilistic time-invariant parametric uncertainties and additive white noises are taken into account by the developed PCE-transformed system. Moreover, the approximation errors introduced by the PCE truncations are captured by time-varying norm-bounded uncertainties whose bound is used as a robustifying tuning parameter. Based on the above PCE-transformed system, a nominal $\mathcal{H}_2$ synthesis approach is proposed when neglecting PCE truncation errors, while a guaranteed cost $\mathcal{H}_2$ control is adopted to cope with PCE truncation errors. The use of a robustifying parameter enforces closed-loop stability without resorting to a high-degree PCE, thus avoiding high computational complexity due to a large number of PCE terms. Moreover, rigorous analysis reveals the relationship between the stability of the PCE-transformed system and the internal mean square stability of the original system under control. Using iterations between synthesis and post-analysis, a bisection algorithm is proposed to find the smallest robustifying parameter that ensures robust closed-loop stability. In contrast, further analysis shows that the Monte-Carlo sampling based $\mathcal{H}_2$ synthesis is much less computationally efficient, and converges to imposing the conservative worst-case stability constraint as the number of samples grows to infinity.

This journal article extends the authors' previous conference paper (Shen et al., 2017) in several ways including robust synthesis that explicitly accounts for PCE truncation errors, dynamic output feedback control synthesis, and providing proofs of the theoretical results.

This paper is organized as follows. Section 2 states the probabilistic robust $\mathcal{H}_2$ control problem. Section 3 reviews preliminaries of PC theory and analyzes the effect of PCE truncation errors. Our proposed static and dynamic output-feedback controls are presented in Sections 4 and 5 , respectively. Section 6 compares our PCE-based approaches to the Monte-Carlo sampling based synthesis. The simulation study and some conclusions are presented in Sections 7 and 8 , respectively.

2. Problem statement

Consider the linear time-invariant (LTI) dynamical system described by

$$\dot{\mathbf{x}}(t,\boldsymbol{\xi}) = \mathbf{A}(\boldsymbol{\xi})\mathbf{x}(t,\boldsymbol{\xi}) + \mathbf{B}_{\mathbf{w}}(\boldsymbol{\xi})\mathbf{w}(t) + \mathbf{B}(\boldsymbol{\xi})\mathbf{u}(t,\boldsymbol{\xi}) \tag{1a}$$

$$\mathbf{z}(t,\boldsymbol{\xi}) = \mathbf{C}_{\mathbf{z}}(\boldsymbol{\xi})\mathbf{x}(t,\boldsymbol{\xi}) + \mathbf{D}_{\mathbf{zw}}\mathbf{w}(t) + \mathbf{D}_{\mathbf{z}}\mathbf{u}(t,\boldsymbol{\xi}) \tag{1b}$$

$$\mathbf{y}(t,\boldsymbol{\xi}) = \mathbf{C}(\boldsymbol{\xi})\mathbf{x}(t,\boldsymbol{\xi}) + \mathbf{D}_{\mathbf{w}}\mathbf{w}(t) \tag{1c}$$

where $\mathbf{x} \in \mathbb{R}^{n_x}$ is the state, $\mathbf{u} \in \mathbb{R}^{n_u}$ is the control input, $\mathbf{w} \in \mathbb{R}^{n_w}$ is the stochastic disturbance or noise, $\mathbf{y} \in \mathbb{R}^{n_y}$ is the measured output, and $\mathbf{z} \in \mathbb{R}^{n_z}$ is the controlled output related to the performance of the control system. Since $\mathbf{A}$, $\mathbf{B_w}$, $\mathbf{B}$, $\mathbf{C}$, and $\mathbf{C_z}$ in (1) are general nonlinear functions of a random parameter vector $\boldsymbol{\xi} \in \mathbb{R}^{n_\xi}$, the system state $\mathbf{x}$, control input $\mathbf{u}$, measured output $\mathbf{y}$, and controlled output $\mathbf{z}$ all depend on $\boldsymbol{\xi}$. Note that $\mathbf{D_{zw}}$ and $\mathbf{D_z}$ in (1b) are assumed to be independent of $\boldsymbol{\xi}$, for the sake of notation simplicity. Note that $\mathbf{D_w}$ in (1c) is assumed to be independent of $\boldsymbol{\xi}$ for the sake of brevity, which is explained later in Remark 3.

The uncertain parameter vector $\boldsymbol{\xi}$ lies within a bounded set Ξ, and its elements are assumed to be mutually independent random variables with known probability density functions (PDFs). The PDF of $\boldsymbol{\xi}$ can be obtained via either offline parameter identification from data, or the a priori knowledge that specifies the relative belief/importance of the underlying system at different points in the uncertainty region Ξ. The above assumption of mutual independence among the elements of $\boldsymbol{\xi}$ is not restrictive, since linear transformation (Rosenblatt, 1952) or Karhunen–Loève expansion (Li & Zhang, 2007) can be applied to remove correlation among these elements. With the above time-invariant probabilistic parametric uncertainties, the system model (1) describes a family of LTI systems associated with a probability measure, i.e., each LTI system with a specific value of $\boldsymbol{\xi}$ is assigned with a relative weight determined by the PDF of $\boldsymbol{\xi}$ (Fisher & Bhattacharya, 2009; Konda et al., 2011; Piga & Benavoli, 2017).

The objective of this paper is to design

(i) a static output-feedback (SOF) controller

$$\mathbf{u}(t,\boldsymbol{\xi}) = \mathbf{K}\mathbf{y}(t,\boldsymbol{\xi}) \tag{2}$$

(ii) a dynamic output-feedback (DOF) controller

$$\begin{aligned}\dot{\mathbf{x}}_K(t,\boldsymbol{\xi}) &= \mathbf{A}_K\mathbf{x}_K(t,\boldsymbol{\xi}) + \mathbf{B}_K\mathbf{y}(t,\boldsymbol{\xi})\\ \mathbf{u}(t,\boldsymbol{\xi}) &= \mathbf{C}_K\mathbf{x}_K(t,\boldsymbol{\xi}) + \mathbf{D}_K\mathbf{y}(t,\boldsymbol{\xi})\end{aligned} \tag{3}$$

that minimizes the $\mathcal{H}_2$ norm of the closed-loop system $\mathcal{T}_{\mathbf{zw}}$ in (1)–(3) from the noisy input $\mathbf{w}$ to the controlled output $\mathbf{z}$. Here, $\mathbf{x}_K \in \mathbb{R}^{n_c}$ and $n_c \le n_x$. To account for the time-invariant probabilistic parametric uncertainties $\boldsymbol{\xi}$, the $\mathcal{H}_2$ norm of the closed-loop system $\mathcal{T}_{\mathbf{zw}}$ in (1)–(3) is defined as

$$\begin{aligned}\|\mathcal{T}_{\mathbf{zw}}\|_2^2 &= \mathbb{E}_{\boldsymbol{\xi}}\left\{\left\|\hat{\mathcal{T}}_{\mathbf{zw}}(\boldsymbol{\xi})\right\|_2^2\right\},\\ \left\|\hat{\mathcal{T}}_{\mathbf{zw}}(\boldsymbol{\xi})\right\|_2^2 &= \sum_{k=1}^{n_w}\int_0^\infty \|\mathbf{z}_k(t,\boldsymbol{\xi})\|_2^2\,\mathrm{d}t,\end{aligned} \tag{4}$$

where $\mathbf{z}_k(t,\boldsymbol{\xi})$ denotes the controlled output response over $t \ge 0$ given the impulse disturbance $\mathbf{w}(t) = \mathbf{e}_k\delta(t)$, with $\delta(t)$ representing the unit impulse and $\mathbf{e}_k$ the kth column of an identity matrix $\mathbf{I}_{n_w}$. As shown in (4), $\|\mathcal{T}_{\mathbf{zw}}\|_2^2$ can be regarded as the averaged squared $\mathcal{H}_2$ norm of a collection of systems $\hat{\mathcal{T}}_{\mathbf{zw}}(\boldsymbol{\xi})$ parameterized by $\boldsymbol{\xi}$. Such a time-domain characterization of the $\mathcal{H}_2$ norm is related to the impulse-to-energy system gain, see Section 4.7 of Skelton et al. (1997). By interchanging the order of expectation, summation and integration, the definition (4) can be rewritten as

$$\|\mathcal{T}_{\mathbf{zw}}\|_2^2 = \sum_{k=1}^{n_w}\int_0^\infty \mathbb{E}_{\boldsymbol{\xi}}\{\|\mathbf{z}_k(t,\boldsymbol{\xi})\|_2^2\}\,\mathrm{d}t. \tag{5}$$

As the usual $\mathcal{H}_2$ norm, the finiteness of $\|\mathcal{T}_{\mathbf{zw}}\|_2^2$ requires $\mathbf{D}_{\mathbf{zw}} + \mathbf{D}_{\mathbf{z}}\mathbf{K}\mathbf{D}_{\mathbf{w}} = \mathbf{0}$ for the SOF case and $\mathbf{D}_{\mathbf{zw}} + \mathbf{D}_{\mathbf{z}}\mathbf{D}_K\mathbf{D}_{\mathbf{w}} = \mathbf{0}$ for the DOF case.

Due to its general nonlinear uncertainty structure, the above problem cannot be effectively addressed by most existing worst-case robust control methods without overbounding the uncertainties. Inspired by Fisher and Bhattacharya (2009) and references therein, the PC theory is adopted to quantify the dependence of $\mathbf{z}_k(t,\boldsymbol{\xi})$ on $\boldsymbol{\xi}$ in the above $\mathcal{H}_2$ norm $\|\mathcal{T}_{\mathbf{zw}}\|_2^2$. Specifically, the substitution of state $\mathbf{x}$, control input $\mathbf{u}$, controlled output $\mathbf{z}$, and measured output $\mathbf{y}$ with their PCE approximations transforms the original stochastic system (1) into a high-dimensional expanded system describing the dynamics of PCE coefficients. The $\mathcal{H}_2$ control synthesis is then solved by using the PCE-transformed system.

The proposed approach aims at improving the existing PCE-based control design methodology by (i) explicitly taking into account stochastic disturbance $\mathbf{w}$; (ii) proposing systematic design procedures to cope with PCE truncation errors which could destabilize the closed-loop system if neglected.

Remark 1. For the sake of notation simplicity, the measured output equation (1c) does not include direct feedthrough. With slight modifications, our proposed PCE-based approach is applicable to direct feedthrough in the two cases:

(i) The DOF control (3) with $\mathbf{D}_K = \mathbf{0}$ can be designed with our proposed PCE-based approach in the presence of direct feedthrough.

(ii) Let $\mathbf{K}_d$ and $\mathbf{K}$ represent the SOF control gains derived with and without direct feedthrough, respectively. Consider the case that the direct feedthrough matrix $\mathbf{D}$ is independent of $\boldsymbol{\xi}$. If $\mathbf{I} + \mathbf{D}\mathbf{K}$ is nonsingular, the relationship $\mathbf{K}_d = \mathbf{K}(\mathbf{I} + \mathbf{D}\mathbf{K})^{-1}$ ensures that the above two controls result in the same closed-loop dynamics (Fletcher, 1981). This approach enables designing $\mathbf{K}_d$ in the presence of direct feedthrough by first computing $\mathbf{K}$ for a system without direct feedthrough.

Other cases that include direct feedthrough and are different from the above two cannot be addressed by the PCE-based approach proposed in this paper, and are left to future research.

3. Polynomial chaos approximation to stochastic linear system

This section provides a brief introduction of polynomial chaos approximation to the stochastic linear system (1) using Galerkin projection, and then shows how the PCE truncation errors affect the PCE-approximated closed-loop dynamics.

3.1. Polynomial chaos expansion

For a random vector $\boldsymbol{\xi}$, a function $\psi(\boldsymbol{\xi}) : \mathbb{R}^{n_\xi} \to \mathbb{R}$ with a finite second-order moment admits a PCE (Xiu, 2010)

$$\psi(\boldsymbol{\xi}) = \sum_{i=0}^{\infty}\psi_i\phi_i(\boldsymbol{\xi}), \tag{6}$$

where $\{\psi_i\}$ denotes the expansion coefficients, and $\{\phi_i(\boldsymbol{\xi})\}$ denotes the multivariate PC bases in terms of $\boldsymbol{\xi}$. By using the Askey scheme of orthogonal polynomial bases, the above expansion exponentially converges in the $\mathcal{L}_2$ sense, which results in accurate approximations even with a relatively small number of terms (Xiu, 2010). These basis functions are orthogonal with respect to the probabilistic distribution $\mu(\boldsymbol{\xi})$ of the random vector $\boldsymbol{\xi}$, i.e., $\phi_0(\boldsymbol{\xi}) = 1$, and

$$\begin{aligned}\langle\phi_i(\boldsymbol{\xi}),\phi_j(\boldsymbol{\xi})\rangle &= \int_\Xi \phi_i(\boldsymbol{\xi})\phi_j(\boldsymbol{\xi})\mu(\boldsymbol{\xi})\,\mathrm{d}\boldsymbol{\xi} = \mathbb{E}_{\boldsymbol{\xi}}\{\phi_i(\boldsymbol{\xi})\phi_j(\boldsymbol{\xi})\}\\ &= \begin{cases}\langle\phi_i^2(\boldsymbol{\xi})\rangle = 1 & \text{if } i = j\\ 0 & \text{otherwise,}\end{cases}\end{aligned} \tag{7}$$

where Ξ is the support of $\mu(\boldsymbol{\xi})$, and $\phi_i(\boldsymbol{\xi})$'s are normalized such that $\langle\phi_i^2(\boldsymbol{\xi})\rangle = 1$.

In practical computations, a PCE with an infinite number of terms (6) needs to be truncated to a finite degree p,

$$\psi(\boldsymbol{\xi}) \approx \hat{\psi}(\boldsymbol{\xi}) = \sum_{i=0}^{N_p}\psi_i\phi_i(\boldsymbol{\xi}). \tag{8}$$

The total number of terms in (8) is $N_p + 1 = \frac{(n_\xi+p)!}{n_\xi!p!}$, depending on the dimension n_ξ of $\boldsymbol{\xi}$ and the highest degree p of the retained polynomials $\{\phi_i(\boldsymbol{\xi})\}_{i=0}^{N_p}$. By using Wiener–Askey orthogonal polynomials according to the PDF of $\boldsymbol{\xi}$, the truncated PCE approximation $\hat{\psi}(\boldsymbol{\xi})$ in (8) converges to $\psi(\boldsymbol{\xi})$ in the mean-square sense (Xiu, 2010; Xiu & Karniadakis, 2002). Roughly speaking, for a function $\psi(\boldsymbol{\xi})$ with a differentiability order m_d, the above PCE approximation error is $O(p^{-m_d})$, which means that the convergence rate is as fast as p^{-m_d} (Xiu, 2010). As such, in general a sufficiently accurate approximation does not require a very high PCE degree.

3.2. Galerkin projection for stochastic linear system

Let $s_i(t,\boldsymbol{\xi})$ denote the ith component of a vector $\mathbf{s}(t,\boldsymbol{\xi}) \in \mathbb{R}^{n_s}$. The scalar $s_i(t,\boldsymbol{\xi})$ is expressed as

$$s_i(t,\boldsymbol{\xi}) = \hat{s}_i(t,\boldsymbol{\xi}) + \tilde{s}_i(t,\boldsymbol{\xi}), \tag{9}$$

where

$$\hat{s}_i(t,\boldsymbol{\xi}) = \sum_{j=0}^{N_p}\pi_{i,j}(t)\phi_j(\boldsymbol{\xi}) \tag{10}$$

is a truncated PCE with a degree p, $\pi_{i,j}(t)$ is the expansion coefficient associated with the PC basis $\phi_j(\xi)$, and $\tilde{s}_i(t,\xi)$ represents the truncation error. Define

$$\begin{aligned}\hat{\mathbf{s}}(t,\xi)&=\begin{bmatrix}\hat{s}_1(t,\xi) & \hat{s}_2(t,\xi) & \cdots & \hat{s}_{n_s}(t,\xi)\end{bmatrix}^\top\in\mathbb{R}^{n_s},\\ \tilde{\mathbf{s}}(t,\xi)&=\begin{bmatrix}\tilde{s}_1(t,\xi) & \tilde{s}_2(t,\xi) & \cdots & \tilde{s}_{n_s}(t,\xi)\end{bmatrix}^\top\in\mathbb{R}^{n_s},\\ \boldsymbol{\pi}_i^\top(t)&=\begin{bmatrix}\pi_{i,0}(t) & \pi_{i,1}(t) & \cdots & \pi_{i,N_p}(t)\end{bmatrix}\in\mathbb{R}^{1\times(N_p+1)},\end{aligned}\tag{11}$$

$$\begin{aligned}\boldsymbol{\phi}(\xi)&=\begin{bmatrix}\phi_0(\xi) & \phi_1(\xi) & \cdots & \phi_{N_p}(\xi)\end{bmatrix}^\top\in\mathbb{R}^{N_p+1},\\ \mathbf{s}_{\mathrm{PCE}}(t)&=\begin{bmatrix}\boldsymbol{\pi}_1(t) & \cdots & \boldsymbol{\pi}_{n_s}(t)\end{bmatrix}\in\mathbb{R}^{(N_p+1)\times n_s}.\end{aligned}\tag{12}$$

Then the PCE approximation $\hat{s}_i(t,\xi)$ in (10) can be compactly written as $\hat{s}_i(t,\xi)=\boldsymbol{\pi}_i^\top(t)\boldsymbol{\phi}(\xi)$, and the vector $\mathbf{s}(t,\xi)=\begin{bmatrix}s_1(t,\xi)\cdots s_{n_s}(t,\xi)\end{bmatrix}^\top$ is expressed as

$$\begin{aligned}\mathbf{s}(t,\xi)&=\hat{\mathbf{s}}(t,\xi)+\tilde{\mathbf{s}}(t,\xi)=\mathbf{s}_{\mathrm{PCE}}^\top(t)\boldsymbol{\phi}(\xi)+\tilde{\mathbf{s}}(t,\xi)\\&=\underbrace{\left(\boldsymbol{\phi}^\top(\xi)\otimes\mathbf{I}_{n_s}\right)}_{\Phi_{\mathbf{s}}^\top(\xi)}\underbrace{\mathrm{vec}\left(\mathbf{s}_{\mathrm{PCE}}^\top(t)\right)}_{\mathbf{S}(t)}+\tilde{\mathbf{s}}(t,\xi)\end{aligned}\tag{13}$$

where $\otimes$ and $\mathrm{vec}(\cdot)$ represent the Kronecker product and the vectorization of a matrix, respectively. In the last equation of (13), the property of the Kronecker product, i.e., $\mathrm{vec}(EFG)=(G^\top\otimes E)\mathrm{vec}(F)$ is applied (Brewer, 1978). With $\mathbf{s}$ representing $\mathbf{x}$, $\mathbf{u}$, $\mathbf{y}$, or $\mathbf{z}$, the PCE coefficient vectors $\mathbf{X}$, $\mathbf{U}$, $\mathbf{Y}$, and $\mathbf{Z}$ are defined similarly as $\mathbf{S}$ in (13).

With (9)–(13), two equations

$$\mathbb{E}_\xi\{\Phi_{\mathbf{s}}(\xi)\Phi_{\mathbf{s}}^\top(\xi)\}=\mathbf{I}_{n_s(N_p+1)},\ \mathbb{E}_\xi\{\Phi_{\mathbf{s}}(\xi)\tilde{\mathbf{s}}(t,\xi)\}=\mathbf{0}\tag{14}$$

are obtained as a result of the normalized orthogonality of the PC bases in (7). The second equation in (14) is derived from

$$\dot{\tilde{s}}_i(t,\xi)=\frac{d}{dt}\left\{s_i(t,\xi)-\hat{s}_i(t,\xi)\right\}=\sum_{j=N_p+1}^{\infty}\dot{\pi}_{i,j}(t)\phi_j(\xi),$$

$$\mathbb{E}_\xi\{\phi_k(\xi)\dot{\tilde{s}}_i(t,\xi)\}=0,\ k=0,1,\ldots,N_p.$$

In the Galerkin projection, the PCEs of $\mathbf{x}(t,\xi)$ and $\mathbf{u}(t,\xi)$ in the form of (13) are inserted into (1a) to give

$$\begin{aligned}\Phi_{\mathbf{x}}^\top(\xi)\dot{\mathbf{X}}(t)&=\mathbf{A}(\xi)\Phi_{\mathbf{x}}^\top(\xi)\mathbf{X}(t)+\mathbf{B}_{\mathbf{w}}(\xi)\mathbf{w}(t)\\&\quad+\mathbf{B}(\xi)\Phi_{\mathbf{u}}^\top(\xi)\mathbf{U}(t)+\mathbf{r}_{\mathbf{x}}(t,\xi)-\dot{\tilde{\mathbf{x}}}(t,\xi),\end{aligned}\tag{15}$$

$$\mathbf{r}_{\mathbf{x}}(t,\xi)=\mathbf{A}(\xi)\tilde{\mathbf{x}}(t,\xi)+\mathbf{B}(\xi)\tilde{\mathbf{u}}(t,\xi),\tag{16}$$

where $\mathbf{x}(t,\xi)$ and $\mathbf{u}(t,\xi)$ in (1a) are replaced by $\Phi_{\mathbf{x}}^\top(\xi)\mathbf{X}(t)+\tilde{\mathbf{x}}(t,\xi)$ and $\Phi_{\mathbf{u}}^\top(\xi)\mathbf{U}(t)+\tilde{\mathbf{u}}(t,\xi)$, respectively. Note that the error term $\mathbf{r}_{\mathbf{x}}(t,\xi)-\dot{\tilde{\mathbf{x}}}(t,\xi)$ results from the PCE truncation errors $\tilde{\mathbf{x}}(t,\xi)$ and $\tilde{\mathbf{u}}(t,\xi)$. Then, left multiplying (15) by $\Phi_{\mathbf{x}}(\xi)$ gives

$$\begin{aligned}\Phi_{\mathbf{x}}(\xi)\Phi_{\mathbf{x}}^\top(\xi)\dot{\mathbf{X}}(t)&=\Phi_{\mathbf{x}}(\xi)\mathbf{A}(\xi)\Phi_{\mathbf{x}}^\top(\xi)\mathbf{X}(t)\\&\quad+\Phi_{\mathbf{x}}(\xi)\mathbf{B}_{\mathbf{w}}(\xi)\mathbf{w}(t)+\Phi_{\mathbf{x}}(\xi)\mathbf{B}(\xi)\Phi_{\mathbf{u}}^\top(\xi)\mathbf{U}(t)\\&\quad+\Phi_{\mathbf{x}}(\xi)\mathbf{r}_{\mathbf{x}}(t,\xi)-\Phi_{\mathbf{x}}(\xi)\dot{\tilde{\mathbf{x}}}(t,\xi).\end{aligned}\tag{17}$$

By taking the expectation with respect to ξ on both sides of (17), it follows that the PCE-transformed system

$$\dot{\mathbf{X}}(t)=\mathcal{A}\mathbf{X}(t)+\mathcal{B}_{\mathbf{w}}\mathbf{w}(t)+\mathcal{B}\mathbf{U}(t)+\mathbf{R}_{\mathbf{x}}(t)\tag{18}$$

describes the dynamics of the PCE coefficient vector $\mathbf{X}(t)$, with

$$\mathcal{A}=\mathbb{E}_\xi\{\Phi_{\mathbf{x}}(\xi)\mathbf{A}(\xi)\Phi_{\mathbf{x}}^\top(\xi)\},\tag{19a}$$

$$\mathcal{B}_{\mathbf{w}}=\mathbb{E}_\xi\{\Phi_{\mathbf{x}}(\xi)\mathbf{B}_{\mathbf{w}}(\xi)\},\tag{19b}$$

$$\mathcal{B}=\mathbb{E}_\xi\{\Phi_{\mathbf{x}}(\xi)\mathbf{B}(\xi)\Phi_{\mathbf{u}}^\top(\xi)\},\tag{19c}$$

$$\mathbf{R}_{\mathbf{x}}(t)=\mathbb{E}_\xi\{\Phi_{\mathbf{x}}(\xi)\mathbf{r}_{\mathbf{x}}(t,\xi)\}.\tag{19d}$$

For deriving (18) and (19), (14) is applied. Note that $\mathcal{A}$, $\mathcal{B}_{\mathbf{w}}$, and $\mathcal{B}$ are time-invariant matrices, while $\mathbf{R}_{\mathbf{x}}(t)$ is a time-varying error term since the error term $\mathbf{r}_{\mathbf{x}}(t,\xi)$ is not orthogonal to the low-degree PC bases in $\Phi_{\mathbf{x}}(\xi)$.

Following similar procedures, the controlled output equation (1b), the measured output equation (1c), the SOF controller (2), and the DOF controller (3) can be transformed into

- the PCE-transformed controlled output equation

$$\mathbf{Z}(t)=\mathcal{C}_{\mathbf{Z}}\mathbf{X}(t)+\mathcal{D}_{\mathbf{Zw}}\mathbf{w}(t)+\mathcal{D}_{\mathbf{Z}}\mathbf{U}(t),\tag{20}$$

- the PCE-transformed measured output equation

$$\mathbf{Y}(t)=\mathcal{C}\mathbf{X}(t)+\mathcal{D}_{\mathbf{w}}\mathbf{w}(t)+\mathbf{R}_{\mathbf{y}}(t),\tag{21}$$

- the PCE-transformed SOF controller

$$\mathbf{U}(t)=\mathcal{K}\mathbf{Y}(t),\tag{22}$$

- the PCE-transformed DOF controller

$$\begin{aligned}\dot{\mathbf{X}}_K(t)&=\mathcal{A}_K\mathbf{X}_K(t)+\mathcal{B}_K\mathbf{Y}(t)\\\mathbf{U}(t)&=\mathcal{C}_K\mathbf{X}_K(t)+\mathcal{D}_K\mathbf{Y}(t),\end{aligned}\tag{23}$$

respectively, where

$$\mathcal{C}_{\mathbf{Z}}=\mathbb{E}_\xi\{\Phi_{\mathbf{z}}(\xi)\mathbf{C}_{\mathbf{z}}(\xi)\Phi_{\mathbf{x}}^\top(\xi)\},\ \mathcal{D}_{\mathbf{Zw}}=\mathbb{E}_\xi\{\Phi_{\mathbf{z}}(\xi)\mathbf{D}_{\mathbf{zw}}\},\tag{24a}$$

$$\mathcal{D}_{\mathbf{Z}}=\mathbf{I}_{N_p+1}\otimes\mathbf{D}_{\mathbf{z}},\ \mathcal{C}=\mathbb{E}_\xi\{\Phi_{\mathbf{y}}(\xi)\mathbf{C}(\xi)\Phi_{\mathbf{x}}^\top(\xi)\},\tag{24b}$$

$$\mathcal{D}_{\mathbf{w}}=\mathbb{E}_\xi\{\Phi_{\mathbf{y}}(\xi)\mathbf{D}_{\mathbf{w}}\},\ \mathcal{K}=\mathbf{I}_{N_p+1}\otimes\mathbf{K},\tag{24c}$$

$$\mathcal{A}_K=\mathbf{I}_{N_p+1}\otimes\mathbf{A}_K,\ \mathcal{B}_K=\mathbf{I}_{N_p+1}\otimes\mathbf{B}_K,\tag{24d}$$

$$\mathcal{C}_K=\mathbf{I}_{N_p+1}\otimes\mathbf{C}_K,\ \mathcal{D}_K=\mathbf{I}_{N_p+1}\otimes\mathbf{D}_K,\tag{24e}$$

$\mathbf{R}_{\mathbf{y}}(t)$ is an error term defined as

$$\mathbf{R}_{\mathbf{y}}(t)=\mathbb{E}_\xi\{\Phi_{\mathbf{y}}(\xi)\mathbf{r}_{\mathbf{y}}(t,\xi)\},\ \mathbf{r}_{\mathbf{y}}(t,\xi)=\mathbf{C}(\xi)\tilde{\mathbf{x}}(t,\xi)\tag{25}$$

due to the PCE truncation errors, similar to $\mathbf{R}_{\mathbf{x}}(t)$ in (19d). Note that the matrices in the controlled output equation (1b), the SOF controller (2), and the DOF controller (3) do not depend on ξ, thus the high-degree terms of these equations satisfy $\mathbb{E}_\xi\{\Phi_{\mathbf{s}}(\xi)\tilde{\mathbf{s}}(t,\xi)\}=\mathbf{0}$, where $\mathbf{s}$ represents $\mathbf{x}$, $\mathbf{u}$, $\mathbf{y}$, and $\mathbf{z}$.

As the uncertain system (1) has general nonlinear uncertainty structure depending on ξ, the matrices $\mathcal{A}$, $\mathcal{B}_{\mathbf{w}}$, $\mathcal{B}$, $\mathcal{C}_{\mathbf{Z}}$, $\mathcal{D}_{\mathbf{Zw}}$, $\mathcal{D}_{\mathbf{Z}}$, $\mathcal{C}$, and $\mathcal{D}_{\mathbf{w}}$ defined in (19), (24a), (24b), and (24c) are time-invariant, and can be obtained via numerical integration (Xiu, 2010).

3.3. Error analysis of PCE-approximated dynamics

Most existing PCE-based control design methods, e.g., Fisher and Bhattacharya (2009), relied on the PCE-transformed system (18)–(23) but neglected the error terms $\mathbf{R}_{\mathbf{x}}(t)$ and $\mathbf{R}_{\mathbf{y}}(t)$ therein. In this case, even though the PCE-transformed system is stabilized, the closed-loop system might be unstable due to perturbations from the neglected error terms $\mathbf{R}_{\mathbf{x}}(t)$ and $\mathbf{R}_{\mathbf{y}}(t)$, as is analyzed in next section.

Combining the PCE-transformed open-loop dynamics (18) and the PCE-transformed SOF controller (22) gives the PCE-transformed closed-loop system

$$\begin{aligned}\dot{\mathbf{X}}(t)&=\left(\mathcal{A}+\mathcal{B}\mathcal{K}\mathcal{C}\right)\mathbf{X}(t)+\left(\mathcal{B}_{\mathbf{w}}+\mathcal{B}\mathcal{K}\mathcal{D}_{\mathbf{w}}\right)\mathbf{w}(t)\\&\quad+\mathbf{R}_{\mathbf{x}}(t)+\mathcal{B}\mathcal{K}\mathbf{R}_{\mathbf{y}}(t)\\\mathbf{Z}(t)&=\left(\mathcal{C}_{\mathbf{Z}}+\mathcal{D}_{\mathbf{Z}}\mathcal{K}\mathcal{C}\right)\mathbf{X}(t)+\left(\mathcal{D}_{\mathbf{Zw}}+\mathcal{D}_{\mathbf{Z}}\mathcal{K}\mathcal{D}_{\mathbf{w}}\right)\mathbf{w}(t)\\&\quad+\mathcal{D}_{\mathbf{Z}}\mathcal{K}\mathbf{R}_{\mathbf{y}}(t).\end{aligned}\tag{26}$$

To facilitate the PCE-based control synthesis, the following expressions for the two error terms $\mathbf{R}_{\mathbf{x}}(t)$ and $\mathbf{R}_{\mathbf{y}}(t)$ are derived, with a proof given in Appendix A.

Proposition 1. *There exist time-varying matrices $\mathcal{F}_{\mathbf{x}}(t)$ and $\mathcal{F}_{\mathbf{y}}(t)$ such that*

$$\mathbf{R}_{\mathbf{x}}(t)=\mathcal{F}_{\mathbf{x}}(t)\mathbf{X}(t),\ \mathbf{R}_{\mathbf{y}}(t)=\mathcal{F}_{\mathbf{y}}(t)\mathbf{X}(t).\tag{27}$$

Using the above notations, the PCE-transformed closed-loop system (26) can be written as

$$\mathcal{T}_{\mathbf{zw}} = \left[\begin{array}{c|c} \mathcal{A}+\mathcal{B}\mathcal{K}\mathcal{C}+\mathcal{F}_{\mathbf{x}}(t)+\mathcal{B}\mathcal{K}\mathcal{F}_{\mathbf{y}}(t) & \mathcal{B}_{\mathbf{w}}+\mathcal{B}\mathcal{K}\mathcal{D}_{\mathbf{w}} \\ \hline \mathcal{C}_{\mathbf{z}}+\mathcal{D}_{\mathbf{z}}\mathcal{K}\mathcal{C}+\mathcal{D}_{\mathbf{z}}\mathcal{K}\mathcal{F}_{\mathbf{y}}(t) & \mathcal{D}_{\mathbf{zw}}+\mathcal{D}_{\mathbf{z}}\mathcal{K}\mathcal{D}_{\mathbf{w}} \end{array}\right]. \tag{28}$$

With similar procedures, the PCE-transformed closed-loop system under the PCE-transformed DOF controller (23) is

$$\bar{\mathcal{T}}_{\mathbf{zw}} = \left[\begin{array}{cc|c} \mathcal{A}+\mathcal{B}\mathcal{D}_K\mathcal{C}+\mathcal{F}_{\mathbf{x}}(t)+\mathcal{B}\mathcal{D}_K\mathcal{F}_{\mathbf{y}}(t) & \mathcal{B}\mathcal{C}_K & \mathcal{B}_{\mathbf{w}}+\mathcal{B}\mathcal{D}_K\mathcal{D}_{\mathbf{w}} \\ \mathcal{B}_K\mathcal{C}+\mathcal{B}_K\mathcal{F}_{\mathbf{y}}(t) & \mathcal{A}_K & \mathcal{B}_K\mathcal{D}_{\mathbf{w}} \\ \hline \mathcal{C}_{\mathbf{z}}+\mathcal{D}_{\mathbf{z}}\mathcal{D}_K\mathcal{C}+\mathcal{D}_{\mathbf{z}}\mathcal{D}_K\mathcal{F}_{\mathbf{y}}(t) & \mathcal{D}_{\mathbf{z}}\mathcal{C}_K & \mathcal{D}_{\mathbf{zw}}+\mathcal{D}_{\mathbf{z}}\mathcal{D}_K\mathcal{D}_{\mathbf{w}} \end{array}\right]. \tag{29}$$

In (28) and (29), the effect of the PCE truncation errors is described by the multiplicative uncertainties $\mathcal{F}_{\mathbf{x}}(t)$ and $\mathcal{F}_{\mathbf{y}}(t)$. They would destabilize the closed-loop system in certain cases if completely neglected. How to cope with these uncertainties will be discussed in Sections 4.2, 4.3, and 5.

4. Static output-feedback synthesis using polynomial chaos

In this section, two PCE-based $\mathcal{H}_2$ synthesis methods are proposed for the SOF synthesis problem formulated in Section 2, using the PCE-transformed systems (18)–(22). The first PCE-based synthesis method neglects the PCE approximation errors $\mathbf{R}_{\mathbf{x}}(t)$ and $\mathbf{R}_{\mathbf{y}}(t)$ analyzed in Section 3.3, while the second PCE-based synthesis method explicitly copes with these error terms using a guaranteed-cost approach.

4.1. $\mathcal{H}_2$ Static output-feedback synthesis

According to (13), the controlled output $\mathbf{z}(t,\boldsymbol{\xi})$ can be written as

$$\mathbf{z}(t,\boldsymbol{\xi}) = \Phi_{\mathbf{z}}^{\top}(\boldsymbol{\xi})\mathbf{Z}(t) + \tilde{\mathbf{z}}(t,\boldsymbol{\xi}),$$

which leads to

$$\begin{aligned} &\mathbb{E}_{\boldsymbol{\xi}}\{\|\mathbf{z}(t,\boldsymbol{\xi})\|_2^2\} \\ &= \mathbf{Z}^{\top}(t)\mathbb{E}_{\boldsymbol{\xi}}\{\Phi_{\mathbf{z}}(\boldsymbol{\xi})\Phi_{\mathbf{z}}^{\top}(\boldsymbol{\xi})\}\mathbf{Z}(t) \\ &\quad + 2\mathbf{Z}^{\top}(t)\mathbb{E}_{\boldsymbol{\xi}}\{\Phi_{\mathbf{z}}(\boldsymbol{\xi})\tilde{\mathbf{z}}(t,\boldsymbol{\xi})\} + \mathbb{E}_{\boldsymbol{\xi}}\{\left\|\tilde{\mathbf{z}}(t,\boldsymbol{\xi})\right\|_2^2\} \\ &\approx \|\mathbf{Z}(t)\|_2^2. \end{aligned} \tag{30}$$

In the above equation, $\mathbb{E}_{\boldsymbol{\xi}}\left\{\Phi_{\mathbf{z}}(\boldsymbol{\xi})\Phi_{\mathbf{z}}^{\top}(\boldsymbol{\xi})\right\} = \mathbf{I}_{n_z(N_p+1)}$ and $\mathbb{E}_{\boldsymbol{\xi}}\left\{\Phi_{\mathbf{z}}(\boldsymbol{\xi})\tilde{\mathbf{z}}(t,\boldsymbol{\xi})\right\} = \mathbf{0}$ are used as a result of the normalized orthogonality (7). The term $\mathbb{E}_{\boldsymbol{\xi}}\left\{\left\|\tilde{\mathbf{z}}(t,\boldsymbol{\xi})\right\|_2^2\right\}$ due to the PCE truncation error $\tilde{\mathbf{z}}(t,\boldsymbol{\xi})$ is neglected, because it converges to zero at a fast rate, and thus could be sufficiently small without using a high PCE degree, see explanations at the end of Section 3.1. From (30), minimizing the $\mathcal{H}_2$ norm $\|\mathcal{T}_{\mathbf{zw}}\|_2^2$ in (5) can be approximated by

$$\min_{\mathbf{K}} \sum_{k=1}^{n_w} \int_0^{\infty} \|\mathbf{Z}_k(t)\|_2^2 \,\mathrm{d}t, \tag{31}$$

where $\mathbf{Z}_k(t)$ is the PCE coefficient vector of the output response $\mathbf{z}_k(t,\boldsymbol{\xi})$ in (5). By doing so, the original SOF problem (5) of minimizing the $\mathcal{H}_2$ norm $\|\mathcal{T}_{\mathbf{zw}}\|_2^2$ in (5) is transformed into a standard nominal $\mathcal{H}_2$ SOF problem (31) for the linear time-invariant PCE-transformed system (18)–(22), when the error terms $\mathbf{R}_{\mathbf{x}}(t)$ and $\mathbf{R}_{\mathbf{y}}(t)$ can be neglected. How to cope with nonnegligible errors $\mathbf{R}_{\mathbf{x}}(t)$ and $\mathbf{R}_{\mathbf{y}}(t)$ will be discussed in Sections 4.2 and 4.3 .

The problem (31) aims at minimizing the $\mathcal{H}_2$ norm of the PCE-transformed closed-loop system (28) from the disturbance $\mathbf{w}$ to the measured output $\mathbf{Z}$. Note that $\mathcal{F}_{\mathbf{x}}(t)$ and $\mathcal{F}_{\mathbf{y}}(t)$ in (28) are set to zero due to neglecting PCE truncation errors, and $\mathcal{D}_{\mathbf{zw}}+\mathcal{D}_{\mathbf{z}}\mathcal{K}\mathcal{D}_{\mathbf{w}} = \mathbf{0}$ is required to obtain a finite $\mathcal{H}_2$ norm. Then standard procedures are used to convert (31) into the optimization

$$\begin{aligned} &\min_{\mathbf{P}_{\mathrm{cs}},\mathbf{K}} \operatorname{trace}\left(\mathcal{B}_{\mathbf{w},\mathrm{cs}}^{\top}\mathbf{P}_{\mathrm{cs}}\mathcal{B}_{\mathbf{w},\mathrm{cs}}\right) \\ &\text{s.t. } \mathbf{P}_{\mathrm{cs}} > 0,\ \mathcal{A}_{\mathrm{cs}}^{\top}\mathbf{P}_{\mathrm{cs}} + \mathbf{P}_{\mathrm{cs}}\mathcal{A}_{\mathrm{cs}} + \mathcal{C}_{\mathbf{z},\mathrm{cs}}^{\top}\mathcal{C}_{\mathbf{z},\mathrm{cs}} < 0 \end{aligned}$$

where

$$\begin{aligned} &\mathcal{A}_{\mathrm{cs}} = \mathcal{A}+\mathcal{B}\mathcal{K}\mathcal{C}, \qquad \mathcal{B}_{\mathbf{w},\mathrm{cs}} = \mathcal{B}_{\mathbf{w}}+\mathcal{B}\mathcal{K}\mathcal{D}_{\mathbf{w}}, \\ &\mathcal{C}_{\mathbf{z},\mathrm{cs}} = \mathcal{C}_{\mathbf{z}}+\mathcal{D}_{\mathbf{z}}\mathcal{K}\mathcal{C}, \end{aligned} \tag{32}$$

and the subscript "cs" indicates that all three matrices are for the closed-loop system under SOF. The above problem can be equivalently transformed into

$$\begin{aligned} &\min_{\boldsymbol{\Lambda}_{\mathrm{cs}},\mathbf{Q}_{\mathrm{cs}},\mathbf{K}} \operatorname{trace}\left(\mathbf{Q}_{\mathrm{cs}}\right) \\ &\text{s.t. } \begin{bmatrix} \mathbf{Q}_{\mathrm{cs}} & \star \\ \mathcal{B}_{\mathbf{w}}+\mathcal{B}\mathcal{K}\mathcal{D}_{\mathbf{w}} & \boldsymbol{\Lambda}_{\mathrm{cs}} \end{bmatrix} > 0, \\ &\quad \begin{bmatrix} \mathrm{He}\{(\mathcal{A}+\mathcal{B}\mathcal{K}\mathcal{C})\boldsymbol{\Lambda}_{\mathrm{cs}}\} & \star \\ (\mathcal{C}_{\mathbf{z}}+\mathcal{D}_{\mathbf{z}}\mathcal{K}\mathcal{C})\boldsymbol{\Lambda}_{\mathrm{cs}} & -\mathbf{I} \end{bmatrix} < 0, \end{aligned} \tag{33}$$

using $\boldsymbol{\Lambda}_{\mathrm{cs}} = \mathbf{P}_{\mathrm{cs}}^{-1}$, and $\mathcal{K}$ defined in (24c), according to the Schur complement lemma, where $\mathrm{He}\{\cdot\}$ denotes the sum of a square matrix and its transpose. In the rest of this paper, within a symmetric block matrix as in (33), an off-diagonal block $\star$ at the position (i,j) represents the transpose of the block at the symmetric position (j,i). As in any standard SOF problem, the second matrix inequality in (33) is a bilinear matrix inequality (BMI) (VanAntwerp & Braatz, 2000) due to the multiplication between $\boldsymbol{\Lambda}_{\mathrm{cs}}$ and $\mathcal{K}$ as well as the special structure of $\mathcal{K} = \mathbf{I}_{N_p+1}\otimes\mathbf{K}$.

The above $\mathcal{H}_2$ synthesis problem extends the PCE-based linear quadratic regulation method proposed in Fisher and Bhattacharya (2009) to address the additive stochastic disturbance $\mathbf{w}$. This formulation has the same limitation as (Fisher & Bhattacharya, 2009) as a result of neglecting the PCE truncation errors, i.e., the above synthesis might fail to stabilize the original dynamics (1a) (Lucia et al., 2017). Specifically, the accuracy of the PCE approximation degrades over time, and the perturbation from the neglected error terms $\mathbf{R}_{\mathbf{x}}(t)$ and $\mathbf{R}_{\mathbf{y}}(t)$ in the closed-loop system (28) grows (Luchtenburg et al., 2014). When the control action does not provide sufficient compensation for such a model-plant mismatch, the system state would diverge. Few existing PCE-based control designs explicitly address this problem (Lucia et al., 2017). The commonly adopted remedy in literature is the use of higher degree PCE approximations at the cost of larger computational burden when solving (33). As the PCE degree p increases, the number of PCE terms increases factorially, and then the involved computational burden rapidly grows and easily becomes prohibitive.

4.2. $\mathcal{H}_2$ Guaranteed cost static output-feedback synthesis

In order to explicitly compensate for PCE truncation errors in the PCE-based synthesis, the error terms $\mathbf{r}_{\mathbf{x}}(t,\boldsymbol{\xi})$ in (16) and $\mathbf{r}_{\mathbf{y}}(t,\boldsymbol{\xi})$ in (25) are assumed to be bounded as

$$\mathbb{E}_{\boldsymbol{\xi}}\left\{\|\Phi_{\mathbf{s}}(\boldsymbol{\xi})\mathbf{r}_{\mathbf{s}}(t,\boldsymbol{\xi})\|_2^2\right\} \le \rho_{\mathbf{s}}^2 \|\mathbf{X}(t)\|_2^2 \tag{34}$$

where $\mathbf{s}$ represents $\mathbf{x}$ and $\mathbf{y}$, respectively. From (19d), (25) and (34), it then follows that

$$\begin{aligned} \|\mathbf{R}_{\mathbf{s}}(t)\|_2^2 &= \left\|\mathbb{E}_{\boldsymbol{\xi}}\left\{\Phi_{\mathbf{s}}(\boldsymbol{\xi})\mathbf{r}_{\mathbf{s}}(t,\boldsymbol{\xi})\right\}\right\|_2^2 \\ &\le \mathbb{E}_{\boldsymbol{\xi}}\left\{\|\Phi_{\mathbf{s}}(\boldsymbol{\xi})\mathbf{r}_{\mathbf{s}}(t,\boldsymbol{\xi})\|_2^2\right\} \le \rho_{\mathbf{s}}^2 \|\mathbf{X}(t)\|_2^2, \end{aligned}$$

and consequently, $\mathcal{F}_{\mathbf{s}}^{\top}(t)\mathcal{F}_{\mathbf{s}}(t) \leq \rho_{\mathbf{s}}^2\mathbf{I}_{n_x(N_p+1)}$ according to (27). With the above norm-bounded uncertainty description of $\mathcal{F}_{\mathbf{x}}(t)$ and $\mathcal{F}_{\mathbf{y}}(t)$, the synthesis of the PCE-transformed closed-loop system (28) is proposed below, with tuning of $\rho_{\mathbf{x}}$ and $\rho_{\mathbf{y}}$ discussed in Section 4.3.

First, the PCE-transformed closed-loop system (28) is rewritten as

$$\dot{\mathbf{X}}(t) = \mathcal{A}_{\text{cs}}\mathbf{X}(t) + \mathcal{G}_{\text{cs}}\boldsymbol{\omega}_{\text{cs}}(t) + \mathcal{B}_{\mathbf{w},\text{cs}}\mathbf{w}(t) \tag{35a}$$

$$\mathbf{Z}(t) = \mathcal{C}_{\mathbf{Z},\text{cs}}\mathbf{X}(t) + \mathcal{L}_{\text{cs}}\boldsymbol{\omega}_{\text{cs}}(t) \tag{35b}$$

$$\boldsymbol{\omega}_{\text{cs}}(t) = \begin{bmatrix} \boldsymbol{\Delta}_{\mathbf{x}}(t) & \mathbf{0} \\ \mathbf{0} & \boldsymbol{\Delta}_{\mathbf{y}}(t) \end{bmatrix} \boldsymbol{\psi}_{\text{cs}}(t), \tag{35c}$$

$$\boldsymbol{\psi}_{\text{cs}}(t) = \begin{bmatrix} \rho_{\mathbf{x}}\mathbf{I} \\ \rho_{\mathbf{y}}\mathbf{I} \end{bmatrix} \mathbf{X}(t), \tag{35d}$$

with $\mathcal{A}_{\text{cs}}$, $\mathcal{B}_{\mathbf{w},\text{cs}}$, and $\mathcal{C}_{\mathbf{Z},\text{cs}}$ defined in (32), and

$$\mathcal{G}_{\text{cs}} = \begin{bmatrix} \mathbf{I} & \mathcal{B}\mathcal{K} \end{bmatrix}, \ \mathcal{L}_{\text{cs}} = \begin{bmatrix} \mathbf{0} & \mathcal{D}_{\mathbf{Z}}\mathcal{K} \end{bmatrix}, \tag{36}$$

$$\boldsymbol{\Delta}_{\mathbf{s}}(t) = \frac{\mathcal{F}_{\mathbf{s}}(t)}{\rho_{\mathbf{s}}}, \ \|\boldsymbol{\Delta}_{\mathbf{s}}(t)\| \leq 1, \ \mathbf{s} \text{ presents } \mathbf{x} \text{ or } \mathbf{y}. \tag{37}$$

With the same procedures in Section 4.1, the design objective (5) is transformed into (31).

Theorem 1. *The closed-loop system (35) is quadratically stable for all $\|\Delta_{\mathbf{x}}(t)\| \leq 1$ and $\|\Delta_{\mathbf{y}}(t)\| \leq 1$ if and only if there exist $\mathbf{P}_{\text{cs}} > 0$ and a scalar $\mu_{\text{cs}} > 0$ such that*

$$\begin{bmatrix} \mathcal{A}_{\text{cs}}^{\top}\mathbf{P}_{\text{cs}} + \mathbf{P}_{\text{cs}}\mathcal{A}_{\text{cs}} + \mu_{\text{cs}}(\rho_{\mathbf{x}}^2 + \rho_{\mathbf{y}}^2)\mathbf{I} & \star \\ \mathcal{G}_{\text{cs}}^{\top}\mathbf{P}_{\text{cs}} & -\mu_{\text{cs}}\mathbf{I} \end{bmatrix} + \begin{bmatrix} \mathcal{C}_{\mathbf{Z},\text{cs}}^{\top} \\ \mathcal{L}_{\text{cs}}^{\top} \end{bmatrix} \begin{bmatrix} \mathcal{C}_{\mathbf{Z},\text{cs}} & \mathcal{L}_{\text{cs}} \end{bmatrix} < 0. \tag{38}$$

Suppose the above statement holds, then the $\mathcal{H}_2$ cost function (31) is upper bounded by $\text{trace}\left(\mathcal{B}_{\mathbf{w},\text{cs}}^{\top}\mathbf{P}_{\text{cs}}\mathcal{B}_{\mathbf{w},\text{cs}}\right)$.

The proof is given in Appendix B.

According to Theorem 1, the robust $\mathcal{H}_2$ control synthesis is formulated as

$$\begin{aligned} \min_{\mathbf{P}_{\text{cs}},\mathbf{Q}_{\text{cs}}\mathbf{K},\mu_{\text{cs}}} \quad & \text{trace}\,(\mathbf{Q}_{\text{cs}}) \\ \text{s.t.} \quad & \begin{bmatrix} \mathbf{Q}_{\text{cs}} & \star \\ \mathbf{P}_{\text{cs}}(\mathcal{B}_{\mathbf{w}} + \mathcal{B}\mathcal{K}\mathcal{D}_{\mathbf{w}}) & \mathbf{P}_{\text{cs}} \end{bmatrix} > 0, \\ & \begin{bmatrix} \text{He}\{\mathbf{P}_{\text{cs}}(\mathcal{A} + \mathcal{B}\mathcal{K}\mathcal{C})\} + \mu_{\text{cs}}\rho^2\mathbf{I} & \star & \star & \star \\ \mathbf{P}_{\text{cs}} & -\mu_{\text{cs}}\mathbf{I} & \star & \star \\ \mathcal{K}^{\top}\mathcal{B}^{\top}\mathbf{P}_{\text{cs}} & \mathbf{0} & -\mu_{\text{cs}}\mathbf{I} & \star \\ \mathcal{C}_{\mathbf{Z}} + \mathcal{D}_{\mathbf{Z}}\mathcal{K}\mathcal{C} & \mathbf{0} & \mathcal{D}_{\mathbf{Z}}\mathcal{K} & -\mathbf{I} \end{bmatrix} < 0 \end{aligned} \tag{39}$$

with $\rho^2 = \rho_{\mathbf{x}}^2 + \rho_{\mathbf{y}}^2$. It aims at minimizing an upper bound of the averaged squared $\mathcal{H}_2$ norm. In contrast, the conventional worst-case robust approach minimizes an upper bound of the worst-case squared $\mathcal{H}_2$ norm. Similarly to the second inequality in (33), both inequalities in (39) are BMIs.

4.3. Post-analysis of stability and parameter tuning

The PCE-based synthesis problem (39) relies on a PCE-transformed approximation (35) of the original system (1) under control (2), and explicitly takes into account the PCE approximation errors by introducing the lumped robustifying parameter ρ^2. However, the synthesis solution to (39) might fail to stabilize the original system (1), if the adopted value of ρ^2 is not large enough to ensure $\rho^2 \geq \rho_{\mathbf{x}}^2 + \rho_{\mathbf{y}}^2$, where $\rho_{\mathbf{x}}^2$ and $\rho_{\mathbf{y}}^2$ are defined in (34) to bound the PCE approximation errors. Therefore, two questions arise:

- Q1 Under which conditions does the control gain obtained from (39) stabilize the original system (1);
- Q2 How to systematically tune the lumped robustifying parameter ρ^2 in (39).

The following theorem answers Q1, and will be used to provide the answer to Q2.

Theorem 2. *Assume that for all $\boldsymbol{\xi} \in \Xi$, $(\mathbf{A}(\boldsymbol{\xi}), \mathbf{C}(\boldsymbol{\xi}))$ is detectable, and the matrices $\mathbf{A}(\boldsymbol{\xi})$, $\mathbf{B}(\boldsymbol{\xi})$ and $\mathbf{C}(\boldsymbol{\xi})$ are bounded. With $\rho_{\mathbf{x}}^2$ and $\rho_{\mathbf{y}}^2$ defined in (34) for PCE approximation errors, if the synthesis problem (39) with the robustifying parameter $\rho^2 \geq \rho_{\mathbf{x}}^2 + \rho_{\mathbf{y}}^2$ is feasible, then the obtained controller internally stabilizes the original system (1) in the mean-square sense.*

The proof is given in Appendix C.

Theorem 2 clarifies sufficient conditions for stabilizing the original system (1) with the control gain obtained from (39). One of these sufficient conditions is $\rho^2 \geq \rho_{\mathbf{x}}^2 + \rho_{\mathbf{y}}^2$. However, it is difficult to determine such ρ^2 before a control law is designed, because the error bounds $\rho_{\mathbf{x}}^2$ and $\rho_{\mathbf{y}}^2$ in (34) depend on the control gain $\mathbf{K}$ that is to be designed. To be specific, $\mathbf{r}_{\mathbf{x}}(t,\boldsymbol{\xi})$ and $\mathbf{r}_{\mathbf{y}}(t,\boldsymbol{\xi})$ in (34) describe the errors of the PCE-transformed approximation to the entire closed-loop system, hence must rely on the control gain $\mathbf{K}$. As indicated by (A.5) and (25), $\mathbf{r}_{\mathbf{x}}(t,\boldsymbol{\xi})$ has an explicit dependence on $\mathbf{K}$, and $\mathbf{r}_{\mathbf{y}}(t,\boldsymbol{\xi})$ depends on $\tilde{\mathbf{x}}(t,\boldsymbol{\xi})$ that is related to $\mathbf{r}_{\mathbf{x}}(t,\boldsymbol{\xi})$ and $\mathbf{K}$. Even with a synthesized control gain, it would be still extremely challenging, if not impossible, to verify (34) over an infinite time horizon, because the expressions (A.1) and (A.5) for $\tilde{\mathbf{x}}(t,\boldsymbol{\xi})$ and $\mathbf{r}_{\mathbf{x}}(t,\boldsymbol{\xi})$ cannot be directly evaluated.

Due to the reasons mentioned above, instead of checking whether the sufficient condition $\rho^2 \geq \rho_{\mathbf{x}}^2 + \rho_{\mathbf{y}}^2$ holds, we perform a posterior stability test after solving (39) with a selected ρ^2. Since a small value of ρ^2 is preferred to avoid conservatism, an iterative tuning method is developed to find the least conservative value of ρ^2 such that the controller obtained from (39) stabilizes the system (1). Here, the posterior stability test is performed by using the probabilistic approach of Piga and Benavoli (2017). This approach formulates the robust stability analysis problem in the probabilistic setting, and uses a theory-of-moments relaxation to derive a semidefinite program that computes an upper probability bound of instability. Using only the support information of the probability measure of $\boldsymbol{\xi}$ in the moment relaxation problem, if the derived upper probability bound of instability for all probability measures with the given support is strictly smaller than 1, then robust closed-loop stability is guaranteed according to Property 1 in Piga and Benavoli (2017).

With a selected PCE degree p, the procedure of the PCE-based control synthesis is summarized as follows. Firstly, the nominal PCE-based synthesis (33) is solved. If the posterior stability test shows that the resulting closed-loop system is robustly stable, a stabilizing PCE-based control is found. Otherwise, the robust PCE-based synthesis (39) has to be considered. Together with the posterior stability test, the bisection search described in Algorithm 1 is developed to iteratively tune ρ^2 within an interval $[0, \rho_{\text{max}}^2]$ until its least conservative value ρ_{min}^2 is found. Here, ρ_{max}^2 is the maximal value of ρ^2 that ensures the feasibility of (39), which can be found by another simple bisection search algorithm that is omitted here due to space limit. As such, ρ_{max}^2 has the following two properties according to Theorem 2: i) $\rho_{\text{max}}^2 \geq \rho_{\mathbf{x}}^2 + \rho_{\mathbf{y}}^2$ holds, because Theorem 2 assumes the existence of $\rho^2 \geq \rho_{\mathbf{x}}^2 + \rho_{\mathbf{y}}^2$ that ensures the feasibility of (39); and ii) the solution to (39) with $\rho^2 = \rho_{\text{max}}^2$ stabilizes the original system (1) in the mean-square sense.

Due to the use of the robustifying parameter ρ^2, certain conservativeness is introduced. Such conservatism can be reduced

Algorithm 1 Bisection search for tuning ρ^2 in (39)

Initialization: $\rho_L^2 \leftarrow 0$, $\rho_U^2 \leftarrow \rho_{\max}^2$, where $\rho_{\max}^2$ is the maximal value of ρ^2 that ensures the feasibility of (39). Set the tolerance ϵ of the stopping criteria.
repeat
  $\rho^2 \leftarrow \frac{1}{2}(\rho_L^2 + \rho_U^2)$
  if the posterior robust stability test shows that the solution to (39) with ρ^2 stabilizes the original system (1) **then**
    $\rho_U^2 \leftarrow \rho^2$
  else
    $\rho_L^2 \leftarrow \rho^2$
  end if
until $\rho_U^2 - \rho_L^2 \le \epsilon$
Output: $\rho_{\min}^2 \leftarrow \rho^2$

by moderately increasing the PCE degree p and accordingly reducing ρ^2. This is achieved at the cost of significantly higher computational load, since the size of the synthesis problem grows factorially with the PCE degree.

5. Dynamic output-feedback synthesis using polynomial chaos

In this section, BMI synthesis conditions are derived for the PCE-based $\mathcal{H}_2$ DOF controller by reducing it to a SOF problem, as in the standard DOF synthesis approach proposed in Scherer et al. (1997).

When neglecting the PCE truncation errors, the cost function (31) is considered in the PCE-based DOF synthesis for the PCE-transformed closed-loop system (29), i.e.,

$$\begin{aligned}\bar{\mathcal{T}}_{\mathbf{zw}} &= \left[\begin{array}{c|c} \bar{\mathcal{A}} + \bar{\mathcal{B}}\bar{\mathcal{K}}\bar{\mathcal{C}} & \bar{\mathcal{B}}_{\mathbf{w}} + \bar{\mathcal{B}}\bar{\mathcal{K}}\bar{\mathcal{D}}_{\mathbf{w}} \\ \hline \bar{\mathcal{C}}_{\mathbf{z}} + \bar{\mathcal{D}}_{\mathbf{z}}\bar{\mathcal{K}}\bar{\mathcal{C}} & \bar{\mathcal{D}}_{\mathbf{zw}} + \bar{\mathcal{D}}_{\mathbf{z}}\bar{\mathcal{K}}\bar{\mathcal{D}}_{\mathbf{w}} \end{array}\right] \\ &= \left[\begin{array}{c|c} \mathcal{A}_{\mathrm{cd}} & \mathcal{B}_{\mathbf{w},\mathrm{cd}} \\ \hline \mathcal{C}_{\mathbf{z},\mathrm{cd}} & \mathbf{0} \end{array}\right],\end{aligned} \tag{40}$$

where

$$\begin{aligned}&\bar{\mathcal{A}} = \begin{bmatrix}\mathcal{A} & \mathbf{0}\\ \mathbf{0} & \mathbf{0}\end{bmatrix},\ \bar{\mathcal{B}}_{\mathbf{w}} = \begin{bmatrix}\mathcal{B}_w \\ \mathbf{0}\end{bmatrix},\ \bar{\mathcal{B}} = \begin{bmatrix}\mathcal{B} & \mathbf{0}\\ \mathbf{0} & \mathbf{I}\end{bmatrix},\\ &\bar{\mathcal{C}}_{\mathbf{z}} = \begin{bmatrix}\mathcal{C}_{\mathbf{z}} & \mathbf{0}\end{bmatrix},\ \bar{\mathcal{D}}_{\mathbf{zw}} = \mathcal{D}_{\mathbf{zw}},\ \bar{\mathcal{D}}_{\mathbf{z}} = \begin{bmatrix}\mathcal{D}_{\mathbf{z}} & \mathbf{0}\end{bmatrix},\\ &\bar{\mathcal{C}} = \begin{bmatrix}\mathcal{C} & \mathbf{0}\\ \mathbf{0} & \mathbf{I}\end{bmatrix},\ \bar{\mathcal{D}}_{\mathbf{w}} = \begin{bmatrix}\mathcal{D}_{\mathbf{w}} \\ \mathbf{0}\end{bmatrix},\ \bar{\mathcal{K}} = \begin{bmatrix}\mathcal{D}_K & \mathcal{C}_K\\ \mathcal{B}_K & \mathcal{A}_K\end{bmatrix},\end{aligned} \tag{41}$$

$\mathcal{A}_K$, $\mathcal{B}_K$, $\mathcal{C}_K$, $\mathcal{D}_K$ are defined in (24d) and (24e), the subscript "cd" indicates the closed-loop system matrices under DOF, and $\bar{\mathcal{D}}_{\mathbf{zw}} + \bar{\mathcal{D}}_{\mathbf{z}}\bar{\mathcal{K}}\bar{\mathcal{D}}_{\mathbf{w}} = \mathbf{0}$ is required to obtain a finite $\mathcal{H}_2$ norm. Since (40) and (28) are in the same form, the above PCE-based DOF synthesis problem can be constructed similarly to the PCE-based SOF synthesis problem (33), hence the details are omitted.

When addressing the PCE truncation errors, the PCE-transformed closed-loop system (29) can be rewritten as

$$\begin{aligned}\dot{\mathbf{X}}_{\mathrm{cd}}(t) &= \mathcal{A}_{\mathrm{cd}}\mathbf{X}_{\mathrm{cd}}(t) + \mathcal{G}_{\mathrm{cd}}\boldsymbol{\omega}_{\mathrm{cd}}(t) + \mathcal{B}_{\mathbf{w},\mathrm{cd}}\mathbf{w}(t),\\ \mathbf{Z}(t) &= \mathcal{C}_{\mathbf{z},\mathrm{cd}}\mathbf{X}_{\mathrm{cd}}(t) + \mathcal{L}_{\mathrm{cd}}\boldsymbol{\omega}_{\mathrm{cd}}(t),\\ \boldsymbol{\omega}_{\mathrm{cd}}(t) &= \begin{bmatrix}\boldsymbol{\Delta}_{\mathbf{x}}(t) & \mathbf{0}\\ \mathbf{0} & \boldsymbol{\Delta}_{\mathbf{y}}(t)\end{bmatrix}\boldsymbol{\psi}_{\mathrm{cd}}(t),\\ \boldsymbol{\psi}_{\mathrm{cd}}(t) &= \begin{bmatrix}\rho_{\mathbf{x}}\mathbf{I} & \mathbf{0}\\ \rho_{\mathbf{y}}\mathbf{I} & \mathbf{0}\end{bmatrix}\mathbf{X}_{\mathrm{cd}}(t),\end{aligned} \tag{42}$$

by applying the same procedure that derives (35) from (28), with $\mathbf{X}_{\mathrm{cd}}(t) = \left[\mathbf{X}^\top(t) \quad \mathbf{X}_K^\top(t)\right]^\top$, $\mathcal{A}_{\mathrm{cd}}$, $\mathcal{B}_{\mathbf{w},\mathrm{cd}}$, and $\mathcal{C}_{\mathbf{z},\mathrm{cd}}$ defined in (40) and (40), $\Delta_{\mathbf{x}}(t)$ and $\Delta_{\mathbf{y}}(t)$ defined in (37), and

$$\mathcal{G}_{\mathrm{cd}} = \begin{bmatrix}\mathbf{I} & \mathcal{B}\mathcal{D}_K\\ \mathbf{0} & \mathcal{B}_K\end{bmatrix},\ \mathcal{L}_{\mathrm{cd}} = \begin{bmatrix}\mathbf{0} & \mathcal{D}_{\mathbf{z}}\mathcal{D}_K\end{bmatrix}.$$

Then, the robust $\mathcal{H}_2$ DOF synthesis problem for (42) can be constructed by following Theorem 1 that is applied to the closed-loop SOF system (35).

In the conventional output-feedback synthesis, the additional structure in a DOF controller allows the use of congruence transformation and change of variables to obtain a LMI synthesis problem (Scherer et al., 1997). The same strategy, however, does not work for the above PCE-based DOF synthesis problems because of the block-diagonal structure of controller parameters as shown in (24d) and (24e). Therefore, a BMI solver is needed to solve the PCE-based DOF synthesis problems for a full-order or reduced-order controller.

Remark 2. All the proposed PCE-based synthesis problems involve BMIs, thus are nonconvex. Global optimization algorithms exist which are applicable to moderate-sized BMI problems without requiring an initial guess (Goh et al., 1994). For a BMI problem with a large size, a global optimization algorithm is often computationally prohibited, and the alternative are local optimization algorithms such as PENBMI (Kočvara & Stingl, 2012). To find a good initial guess for the local search, various LMI relaxations or iterative LMI algorithms are available for SOF or DOF controls in literature (Sadabadi & Peaucelle, 2016). It should be noted that modifications have to be made to these existing methods to account for the structures of the SOF/DOF control gains $\mathcal{K}$ in (24c) and $\bar{\mathcal{K}}$ in (41). Relevant details are not included here due to limited space. If an initial guess cannot be found by these local search methods, the global search approach can be used by solving a BMI feasibility problem with a higher computational cost.

6. Comparison with Monte-Carlo sampling based $\mathcal{H}_2$ output-feedback synthesis

Following Tempo et al. (2013), a Monte-Carlo sampling based method is briefly reviewed here, to compare with the PCE-based synthesis proposed in the previous sections. For the sake of brevity, only the SOF case is discussed, and similar conclusions are applicable to the DOF case.

When applying the standard $\mathcal{H}_2$ synthesis conditions, the averaged $\mathcal{H}_2$ SOF problem stated in Section 2 can be formulated as

$$\begin{aligned}&\min_{\mathbf{P}(\boldsymbol{\xi}),\mathbf{K}} \mathbb{E}_{\boldsymbol{\xi}}\left\{\mathrm{trace}\left(\mathbf{B}_{\mathbf{w},\mathrm{c}}^\top(\boldsymbol{\xi})\mathbf{P}(\boldsymbol{\xi})\mathbf{B}_{\mathbf{w},\mathrm{c}}(\boldsymbol{\xi})\right)\right\}\\ &\text{s.t. } \mathbf{P}(\boldsymbol{\xi}) > 0,\ \mathbb{E}_{\boldsymbol{\xi}}\left\{\mathbf{x}^\top(t,\boldsymbol{\xi})\boldsymbol{\Upsilon}(\boldsymbol{\xi})\mathbf{x}(t,\boldsymbol{\xi})\right\} < 0,\end{aligned} \tag{43}$$

where $\mathbf{P}(\boldsymbol{\xi}) \in \mathbb{R}^{n_{\mathrm{x}}\times n_{\mathrm{x}}}$ is a predefined function of $\boldsymbol{\xi}$, and

$$\begin{aligned}\mathbf{A}_{\mathrm{c}}(\boldsymbol{\xi}) &= \mathbf{A}(\boldsymbol{\xi}) + \mathbf{B}(\boldsymbol{\xi})\mathbf{K}\mathbf{C}(\boldsymbol{\xi}),\\ \mathbf{B}_{\mathbf{w},\mathrm{c}}(\boldsymbol{\xi}) &= \mathbf{B}_{\mathbf{w}}(\boldsymbol{\xi}) + \mathbf{B}(\boldsymbol{\xi})\mathbf{K}\mathbf{D}_{\mathbf{w}},\\ \mathbf{C}_{\mathbf{z},\mathrm{c}}(\boldsymbol{\xi}) &= \mathbf{C}_{\mathbf{z}}(\boldsymbol{\xi}) + \mathbf{D}_{\mathbf{z}}\mathbf{K}\mathbf{C}(\boldsymbol{\xi}),\\ \boldsymbol{\Upsilon}(\boldsymbol{\xi}) &= \mathbf{A}_{\mathrm{c}}^\top(\boldsymbol{\xi})\mathbf{P}(\boldsymbol{\xi}) + \mathbf{P}(\boldsymbol{\xi})\mathbf{A}_{\mathrm{c}}(\boldsymbol{\xi}) + \mathbf{C}_{\mathbf{z},\mathrm{c}}^\top(\boldsymbol{\xi})\mathbf{C}_{\mathbf{z},\mathrm{c}}(\boldsymbol{\xi}).\end{aligned} \tag{44}$$

The Monte-Carlo sampling based approach uses a finite number of realizations of $\boldsymbol{\xi}$ to recast the above problem as

$$\min_{\substack{\boldsymbol{\Lambda}_1,\ldots,\boldsymbol{\Lambda}_N,\\ \mathbf{Q}_1,\ldots,\mathbf{Q}_N,\mathbf{K}}} \frac{1}{N}\sum_{i=1}^{N}\mathrm{trace}(\mathbf{Q}_i) \tag{45a}$$

$$\text{s.t.} \begin{bmatrix}\boldsymbol{\Lambda}_i\mathbf{A}_{\mathrm{c}}^\top(\boldsymbol{\xi}_i) + \mathbf{A}_{\mathrm{c}}(\boldsymbol{\xi}_i)\boldsymbol{\Lambda}_i & \star\\ \mathbf{C}_{\mathbf{z},\mathrm{c}}(\boldsymbol{\xi}_i)\boldsymbol{\Lambda}_i & -\mathbf{I}\end{bmatrix} < 0, \tag{45b}$$

$$\begin{bmatrix}\mathbf{Q}_i & \star\\ \mathbf{B}_{\mathbf{w},\mathrm{c}}(\boldsymbol{\xi}_i) & \boldsymbol{\Lambda}_i\end{bmatrix} > 0,\ \boldsymbol{\Lambda}_i > 0,\ i = 1,\ldots,N,$$

where $\{\boldsymbol{\xi}_i\}$ are sampled from the probability distribution of $\boldsymbol{\xi}$, N is the number of samples, and each pair of $\boldsymbol{\Lambda}_i$ and $\mathbf{Q}_i$ is applied

to a different sample. The inequalities in (45) are converted from $\mathbf{B}_{\mathbf{w},\mathrm{c}}^{\top}(\boldsymbol{\xi}_i)\mathbf{P}_i\mathbf{B}_{\mathbf{w},\mathrm{c}}(\boldsymbol{\xi}_i) < \mathbf{Q}_i$ and $\boldsymbol{\Upsilon}(\boldsymbol{\xi}_i) < 0$ by using $\boldsymbol{\Lambda}_i = \mathbf{P}_i^{-1}$, with $\boldsymbol{\Upsilon}(\boldsymbol{\xi}_i)$ defined in (44).

To achieve a satisfactory approximation to the original problem (43), a large number of samples are necessary, as analyzed in Sections 8.3 and 10.3 of Tempo et al. (2013). This leads to heavy computational load when solving the problem (45), as illustrated later by a numerical example in Section 7. In contrast, the PCE approximation exponentially converges with its degree increasing, thus usually a relatively small degree is needed. As a result, solving the PCE-based synthesis problems derived in Sections 4 and 5 can be much more efficient. Even when a small PCE degree results in PCE truncation errors to be accounted for, not only the PCE degree p but also the robustifying parameter ρ introduced in Sections 4.2 and 5 are available to enhance our proposed PCE-based design without significantly increasing computational complexity.

Another limitation of the Monte-Carlo sampling based approach lies in replacing the stochastic stability condition $\mathbb{E}_{\boldsymbol{\xi}}\left\{\mathbf{x}^{\top}(t,\boldsymbol{\xi})\boldsymbol{\Upsilon}(\boldsymbol{\xi})\mathbf{x}(t,\boldsymbol{\xi})\right\} < 0$ in (43) by (45a). This is conservative, because (45a) converges to a worst-case robust stability constraint as the sample size increases.

7. Numerical simulations

Consider a system of the form (1) whose parameters are

$$\begin{aligned}
&\mathbf{A}(\xi) = \begin{bmatrix} 0.2+0.3\xi^3 & -0.4 \\ 0.1 & 0.5 \end{bmatrix},\ \mathbf{B}_{\mathbf{w}} = \begin{bmatrix} 0.6 & 0 \\ 0 & 1 \end{bmatrix},\\
&\mathbf{B} = \begin{bmatrix} 0.5 & 0.1 \\ 0.2 & 1 \end{bmatrix},\ \mathbf{C}_{\mathbf{z}} = \begin{bmatrix} \mathbf{I}_2 \\ \mathbf{0}_{2\times 2} \end{bmatrix},\ \mathbf{D}_{\mathbf{z}} = \frac{1}{\sqrt{3}}\begin{bmatrix} \mathbf{0}_{2\times 2} \\ \mathbf{I}_2 \end{bmatrix},\\
&\mathbf{C} = \begin{bmatrix} 0.8 & 0.4 \end{bmatrix},\ \mathbf{D}_{\mathbf{w}} = \mathbf{0}_{1\times 2},\ \mathbf{D}_{\mathbf{zw}} = \mathbf{0}_{4\times 2},
\end{aligned} \tag{46}$$

with the uncertain parameter ξ being uniformly distributed over the interval $[-1, 1]$.

Firstly, four $\mathcal{H}_2$ SOF control synthesis methods are implemented for comparisons: (i) a worst-case robust SOF synthesis that exploits the polytopic uncertainty $\xi^3 \in [-1, 1]$ to overbound the polynomial parametric uncertainty in (46) (Geromel et al., 2007); (ii) our proposed PCE-based nominal SOF synthesis (33); (iii) our proposed PCE-based guaranteed cost SOF synthesis (39); (iv) a Monte-Carlo sampling based SOF synthesis. With the implemented SOF controls, the $\mathcal{H}_2$ norms $\left\|\hat{\mathcal{T}}_{\mathbf{zw}}(\boldsymbol{\xi})\right\|_2$ defined in (4) vary with $\boldsymbol{\xi}$, as depicted in Fig. 1. Both the worst-case robust SOF control and the 10-degree PCE-based nominal SOF control succeed in stabilizing the closed-loop system, whilst the 2-degree PCE-based nominal SOF control fails. It can be also seen that compared to the worst-case robust SOF control, although the 10-degree PCE-based nominal SOF control gives a larger worst-case $\mathcal{H}_2$ norm for $\xi = -1$, it indeed achieves a smaller averaged $\mathcal{H}_2$ norm.

In order to illustrate the benefit of the PCE-based guaranteed cost SOF control synthesis (39), a 2-degree PCE is adopted to introduce relatively larger PCE truncation errors on purpose. The bisection method in Algorithm 1 is applied to find the minimal robustifying parameter $\rho_{\min}$ that results in a robustly stabilizing control gain. First, the lower bound ρ_L and the upper bound ρ_U are chosen as $\rho_L = 0$ and $\rho_U = 9.5 \times 10^{-2}$, respectively. After 11 bisection iterations, the gap between ρ_L and ρ_U becomes smaller than 5×10^{-5}. Then Algorithm 1 terminates, and the minimal robustifying parameter $\rho_{\min}$ is 2.8×10^{-2}. As a result, the obtained SOF gain is $\begin{bmatrix} -21.86 & 16.36 \end{bmatrix}^{\top}$. When performing the posterior stability analysis, the moment relaxation problem of Piga and Benavoli (2017) is formulated with the support information $[-1, 1]$ and the first four orders of moments. The obtained upper probability bound of instability for all probability measures

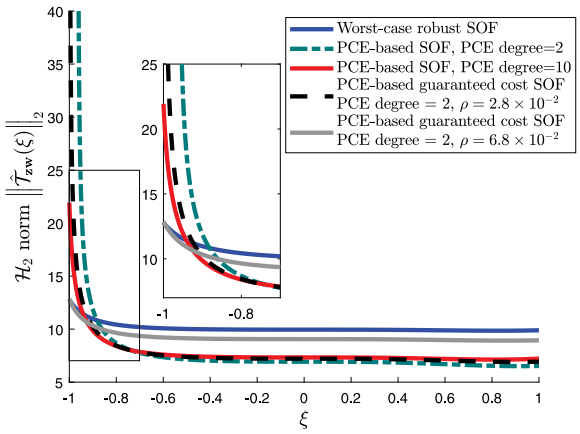

Fig. 1. Variations of the $\mathcal{H}_2$ norm $\left\|\hat{\mathcal{T}}_{\mathbf{zw}}(\boldsymbol{\xi})\right\|_2$ generated by different SOF controls.

with the same support $[-1, 1]$ is 0.00003%, thus robust closed-loop stability is guaranteed according to Property 1 of Piga and Benavoli (2017). In Fig. 1, the 10-degree PCE-based nominal SOF control achieves an averaged $\mathcal{H}_2$ norm 7.7 and a worst-case $\mathcal{H}_2$ norm 21.9. In comparison, the 2-degree PCE-based guaranteed cost SOF control synthesis with $\rho = 2.8 \times 10^{-2}$ results in a similar averaged $\mathcal{H}_2$ norm 8.1, although it obtains a much larger worst-case $\mathcal{H}_2$ norm 289.6. With the robustifying parameter increased to $\rho = 6.8 \times 10^{-2}$, the achieved worst-case $\mathcal{H}_2$ norm is reduced to 12.9, which is almost the same as that of the worst-case robust SOF control, while its averaged $\mathcal{H}_2$ norm has a minor increase to 9.2.

In terms of computational cost, the proposed PCE-based SOF synthesis problems (33) and (39) are compared with the Monte-Carlo sampling based synthesis (45). As shown in Fig. 2, the solution to the Monte-Carlo sampling based formulation (45) converges to $\mathbf{K}_{\mathrm{mc}} = [\,-19.6\ \ 14.9\,]^{\top}$ with 10^4 samples. The number of involved decision variables is 60004. In contrast, both two PCE-based synthesis problems (33) and (39) have a significantly reduced problem size. To be specific, the 10-degree PCE-based nominal SOF synthesis (33) produces almost the same control gain $\mathbf{K}_{\mathrm{PCE}} = [\,-19.5\ \ 14.8\,]^{\top}$ as $\mathbf{K}_{\mathrm{mc}}$, which involves only 508 decision variables. In the 2-degree PCE-based guaranteed cost SOF synthesis (39), the number of decision variables further reduces to 45.

Similarly to the performance comparison of four $\mathcal{H}_2$ SOF controls, the corresponding $\mathcal{H}_2$ DOF controls are also implemented. As depicted in Fig. 3, the results are very similar to Fig. 1. It can be seen again that the 2-degree PCE-based guaranteed cost DOF synthesis with $\rho = 2.5 \times 10^{-2}$ produces almost the same $\mathcal{H}_2$ performance as the 5-degree PCE-based nominal DOF synthesis, but it has a much larger $\mathcal{H}_2$ norm as ξ approaches -1. By increasing ρ to 6.8×10^{-2}, the 2-degree PCE-based guaranteed cost DOF synthesis achieves a slightly smaller worst-case $\mathcal{H}_2$ norm than the worst-case DOF synthesis result. This is due to the conservatism introduced by using polytopic uncertainty description to overbound the polynomial parametric uncertainty in the simulation example (46).

8. Conclusions

Polynomial chaos based $\mathcal{H}_2$ static and dynamic output-feedback control synthesis methods are presented for systems subject to time-invariant probabilistic parametric uncertainties

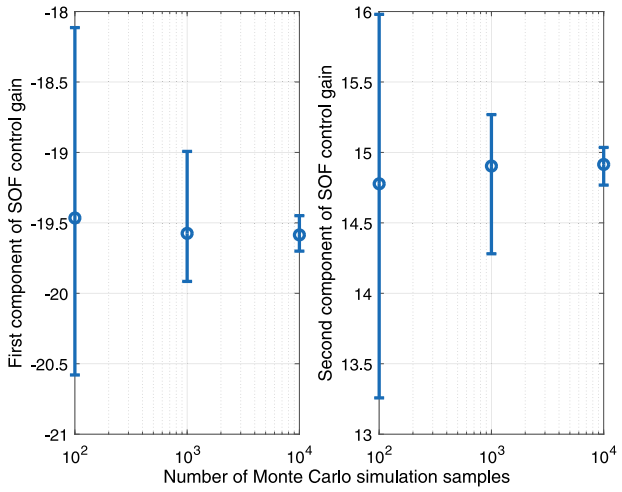

Fig. 2. The dependence of both components of the SOF controller on the number of Monte-Carlo samples (circles: the average of 100 trials with different samples of ξ; error bars: the range of 100 trials). The control gain converges when using 10^4 samples.

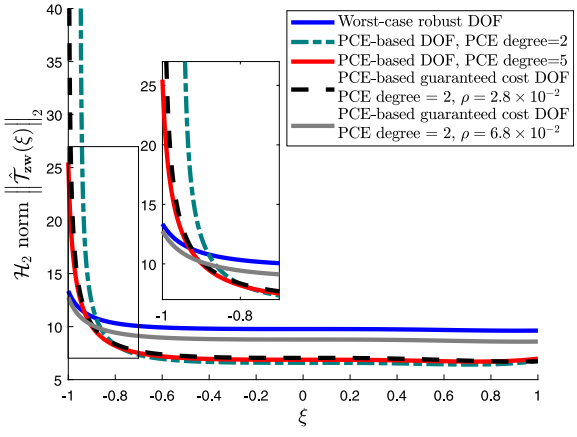

Fig. 3. Variations of the $\mathcal{H}_2$ norm $\left\|\hat{\mathcal{T}}_{\mathbf{zw}}(\xi)\right\|_2$ generated by different DOF controls.

and white noises. The effect of polynomial chaos expansion truncation errors is captured by time-varying norm-bounded uncertainties, and explicitly taken into account by adopting a guaranteed cost control approach. This strategy further leads to rigorous analysis of the condition under which the stability of the PCE-transformed system ensures the closed-loop stability of the original system, which has not been achieved by existing PCE-based controls. Instead of using high-degree expansions to alleviate the effect of truncation errors, our proposed polynomial chaos based synthesis allows the use of relatively low-degree expansions by tuning a robustifying parameter, which significantly reduces computational cost.

Appendix A. Proof of Proposition 1

Between the PCE truncation error $\tilde{\mathbf{x}}(t,\xi)$ and the PCE approximation $\Phi_{\mathbf{x}}^{\top}(\xi)\mathbf{X}(t)$, there exists a non-unique transformation matrix $\mathbf{M}(t,\xi)\in\mathbb{R}^{n_x\times n_x}$ such that

$$\tilde{\mathbf{x}}(t,\xi)=\mathbf{M}(t,\xi)\Phi_{\mathbf{x}}^{\top}(\xi)\mathbf{X}(t) \tag{A.1}$$

holds for all t. Then, it can be derived from (25) and (A.1) that

$$\mathbf{R}_{\mathbf{y}}(t)=\mathbb{E}_{\xi}\{\Phi_{\mathbf{y}}(\xi)\mathbf{C}(\xi)\tilde{\mathbf{x}}(t,\xi)\}=\mathcal{F}_{\mathbf{y}}(t)\mathbf{X}(t) \tag{A.2}$$

with $\mathcal{F}_{\mathbf{y}}(t)=\mathbb{E}_{\xi}\{\Phi_{\mathbf{y}}(\xi)\mathbf{C}(\xi)\mathbf{M}(t,\xi)\Phi_{\mathbf{x}}^{\top}(\xi)\}$.

From (13), (21), (22), and (24c), the truncation error $\tilde{\mathbf{u}}(t,\xi)=\mathbf{u}(t,\xi)-\Phi_{\mathbf{u}}^{\top}(\xi)\mathbf{U}(t)$ can be expressed as

$$\begin{aligned}\tilde{\mathbf{u}}(t,\xi)&=\mathbf{K}\mathbf{y}(t,\xi)-\Phi_{\mathbf{u}}^{\top}(\xi)\mathcal{K}\mathbf{Y}(t)\\&=\mathbf{K}\mathbf{C}(\xi)\left(\Phi_{\mathbf{x}}^{\top}(\xi)\mathbf{X}(t)+\tilde{\mathbf{x}}(t,\xi)\right)+\mathbf{K}\mathbf{D}_{\mathbf{w}}\mathbf{w}(t)\\&\quad-\Phi_{\mathbf{u}}^{\top}(\xi)\mathcal{K}\left(\mathcal{C}\mathbf{X}(t)+\mathcal{D}_{\mathbf{w}}\mathbf{w}(t)+\mathbf{R}_{\mathbf{y}}(t)\right)\\&=\mathbf{K}\mathbf{C}(\xi)\tilde{\mathbf{x}}(t,\xi)-\mathbf{K}\Phi_{\mathbf{y}}^{\top}(\xi)\mathbf{R}_{\mathbf{y}}(t)\\&\quad+\mathbf{K}\left(\mathbf{C}(\xi)\Phi_{\mathbf{x}}^{\top}(\xi)-\Phi_{\mathbf{y}}^{\top}(\xi)\mathcal{C}\right)\mathbf{X}(t).\end{aligned} \tag{A.3}$$

Note that the third equation in (A.3) leverages

$$\Phi_{\mathbf{u}}^{\top}(\xi)\mathcal{K}=\mathbf{K}\Phi_{\mathbf{y}}^{\top}(\xi),\ \ \mathbf{K}\mathbf{D}_{\mathbf{w}}=\Phi_{\mathbf{u}}^{\top}(\xi)\mathcal{K}\mathcal{D}_{\mathbf{w}} \tag{A.4}$$

which are derived by using the definitions of $\Phi_{\mathbf{u}}^{\top}(\xi)$, $\Phi_{\mathbf{y}}^{\top}(\xi)$, $\mathcal{K}$, and $\mathcal{D}_{\mathbf{w}}$ in (13) and (24c) as well as the orthogonality in (7):

$$\begin{aligned}&\Phi_{\mathbf{s}}^{\top}(\xi)=\begin{bmatrix}\mathbf{I}_{n_s} & \phi_1(\xi)\mathbf{I}_{n_s} & \cdots & \phi_{N_p}(\xi)\mathbf{I}_{n_s}\end{bmatrix},\\&\mathcal{D}_{\mathbf{w}}=\mathbb{E}_{\xi}\left\{\left(\boldsymbol{\phi}^{\top}(\xi)\otimes\mathbf{I}_{n_y}\right)\mathbf{D}_{\mathbf{w}}\right\}=\begin{bmatrix}\mathbf{D}_{\mathbf{w}}^{\top} & \mathbf{0}_{n_yN_p\times n_y}\end{bmatrix}^{\top},\end{aligned}$$

where $\mathbf{s}$ represents $\mathbf{u}$ or $\mathbf{y}$. By substituting (A.2), (A.3), and (A.4) into (16), it follows that

$$\begin{aligned}\mathbf{r}_{\mathbf{x}}(t,\xi)&=\mathbf{A}_{\mathrm{cl}}(\xi)\tilde{\mathbf{x}}(t,\xi)-\mathbf{B}(\xi)\mathbf{K}\Phi_{\mathbf{y}}^{\top}(\xi)\mathcal{F}_{\mathbf{y}}(t)\mathbf{X}(t)\\&\quad+\mathbf{B}(\xi)\mathbf{K}\left(\mathbf{C}(\xi)\Phi_{\mathbf{x}}^{\top}(\xi)-\Phi_{\mathbf{y}}^{\top}(\xi)\mathcal{C}\right)\mathbf{X}(t)\end{aligned} \tag{A.5}$$

with $\mathbf{A}_{\mathrm{cl}}(\xi)=\mathbf{A}(\xi)+\mathbf{B}(\xi)\mathbf{K}\mathbf{C}(\xi)$. From the above derivations, $\mathbf{R}_{\mathbf{x}}(t)$ in (19d) can be rewritten as

$$\mathbf{R}_{\mathbf{x}}(t)=\mathbb{E}_{\xi}\{\Phi_{\mathbf{x}}(\xi)\mathbf{r}_{\mathbf{x}}(t,\xi)\}=\mathcal{F}_{\mathbf{x}}(t)\mathbf{X}(t)$$

with

$$\begin{aligned}\mathcal{F}_{\mathbf{x}}(t)&=\mathbb{E}_{\xi}\left\{\Phi_{\mathbf{x}}(\xi)\mathbf{A}_{\mathrm{cl}}(\xi)\mathbf{M}(t,\xi)\Phi_{\mathbf{x}}^{\top}(\xi)\right.\\&\quad-\Phi_{\mathbf{x}}(\xi)\mathbf{B}(\xi)\mathbf{K}\Phi_{\mathbf{y}}^{\top}(\xi)\mathcal{F}_{\mathbf{y}}(t)\\&\quad\left.+\Phi_{\mathbf{x}}(\xi)\mathbf{B}(\xi)\mathbf{K}\left(\mathbf{C}(\xi)\Phi_{\mathbf{x}}^{\top}(\xi)-\Phi_{\mathbf{y}}^{\top}(\xi)\mathcal{C}\right)\right\}.\end{aligned} \tag{A.6}$$

Remark 3. The independence of $\mathbf{D}_{\mathbf{w}}$ on $\boldsymbol{\xi}$ is used for deriving (A.4). Without such an assumption, $\mathbf{R}_{\mathbf{x}}(t)=\mathcal{F}_{\mathbf{x}}(t)\mathbf{X}(t)+\mathcal{F}_{\mathbf{w}}\mathbf{w}(t)$ is then derived with

$$\mathcal{F}_{\mathbf{w}}=\mathbb{E}_{\xi}\left\{\Phi_{\mathbf{x}}(\xi)\mathbf{B}(\xi)\left(\mathbf{K}\mathbf{D}_{\mathbf{w}}(\xi)-\Phi_{\mathbf{u}}^{\top}(\xi)\mathcal{K}\mathcal{D}_{\mathbf{w}}\right)\right\},$$

where $\mathbf{D}_{\mathbf{w}}(\xi)$ depends on $\boldsymbol{\xi}$. In this case, the basic idea for the PCE-based synthesis method in Sections 4.2 and 4.3 is still applicable, except that minor modifications are needed to cope with the additional uncertainty $\mathcal{F}_{\mathbf{w}}\mathbf{w}(t)$. Derivations for this case are not included for the sake of brevity.

Appendix B. Proof of Theorem 1

A sketch of the proof is as follows, and please refer to Section 4.7 in Skelton et al. (1997) for more details. By multiplying (38) with $\begin{bmatrix}\mathbf{X}^{\top}(t) & \boldsymbol{\omega}_{\mathrm{cs}}^{\top}(t)\end{bmatrix}$ to its left and with $\begin{bmatrix}\mathbf{X}^{\top}(t) & \boldsymbol{\omega}_{\mathrm{cs}}^{\top}(t)\end{bmatrix}^{\top}$ to its right, we can derive

$$\begin{aligned}\dot{V}(\mathbf{X}(t))&<-\mathbf{Z}^{\top}(t)\mathbf{Z}(t)\\&\quad+\mu_{\mathrm{cs}}\left(\boldsymbol{\omega}_{\mathrm{cs}}^{\top}(t)\boldsymbol{\omega}_{\mathrm{cs}}(t)-\boldsymbol{\psi}_{\mathrm{cs}}^{\top}(t)\boldsymbol{\psi}_{\mathrm{cs}}(t)\right).\end{aligned} \tag{B.1}$$

from (35), where $V(\mathbf{X}(t))$ is the quadratic Lyapunov function defined as $V(\mathbf{X}(t))=\frac{1}{2}\mathbf{X}^{\top}(t)\mathbf{P}_{\mathrm{cs}}\mathbf{X}(t)$. Since $\|\Delta_{\mathbf{x}}(t)\|\le 1$ and $\left\|\Delta_{\mathbf{y}}(t)\right\|\le 1$, we also have

$$\boldsymbol{\omega}_{\mathrm{cs}}^{\top}(t)\boldsymbol{\omega}_{\mathrm{cs}}(t)-\boldsymbol{\psi}_{\mathrm{cs}}^{\top}(t)\boldsymbol{\psi}_{\mathrm{cs}}(t)\le 0. \tag{B.2}$$

Then, it is easy to see $\dot{V}(\mathbf{X}(t))<0$ from (B.1) and (B.2), which proves the sufficient condition for quadratic stability.

Now, we prove the necessity condition implied by quadratic stability. According to the concept of quadratic stability, there

exists a Lyapunov function $V_1(\mathbf{X}(t)) = \frac{1}{2}\mathbf{X}^\top(t)\mathbf{P}_1\mathbf{X}(t)$ with $\mathbf{P}_1 > 0$ such that $\dot{V}_1(\mathbf{X}(t)) < 0$ holds. Then, using $\dot{V}_1(\mathbf{X}(t)) < 0$ and (B.2), there exist sufficiently small positive scalars ε_1 and ε_2 such that

$$\dot{V}_1(\mathbf{X}(t)) + \varepsilon_1\left(\boldsymbol{\psi}_{\mathrm{cs}}^\top(t)\boldsymbol{\psi}_{\mathrm{cs}}(t) - \boldsymbol{\omega}_{\mathrm{cs}}^\top(t)\boldsymbol{\omega}_{\mathrm{cs}}(t)\right) + \varepsilon_2\mathbf{Z}^\top(t)\mathbf{Z}(t) < 0. \tag{B.3}$$

Dividing both sides of (B.3) by ε_2, and define $\mathbf{P}_{\mathrm{cs}} = \varepsilon_2^{-1}\mathbf{P}_1$ and $\mu_{\mathrm{cs}} = \varepsilon_1\varepsilon_2^{-1}$, we can derive the necessary condition (38) from (B.3) by using (35).

Next, we derive an upper bound for the $\mathcal{H}_2$ cost function (31) by using (B.1) that is obtained from (38). Let $\mathbf{X}_k(t)$, $\mathbf{Z}_k(t)$, $\boldsymbol{\psi}_{\mathrm{cs},k}(t)$, and $\boldsymbol{\omega}_{\mathrm{cs},k}(t)$ denote the impulse responses to the unit-impulse input $\mathbf{w}(t) = \mathbf{e}_k\delta(t)$ in the kth coordinate of $\mathbf{w}$. Integrating both sides of (B.1) from $t = 0$ to ∞ leads to

$$\begin{aligned} V(\mathbf{X}_k(0)) &= V(\mathbf{X}_k(0)) - V(\mathbf{X}_k(\infty)) \\ &> \int_0^\infty \|\mathbf{Z}_k(t)\|_2^2\,dt \\ &\quad + \mu_{\mathrm{cs}}\int_0^\infty \left\|\boldsymbol{\psi}_{\mathrm{cs},k}(t)\right\|_2^2 - \left\|\boldsymbol{\omega}_{\mathrm{cs},k}(t)\right\|_2^2\,dt \\ &\geq \int_0^\infty \|\mathbf{Z}_k(t)\|_2^2\,dt, \end{aligned}$$

In the above derivation, the first equality is due to $V(\mathbf{X}_k(\infty)) = 0$ implied by the quadratic stability, while the second inequality comes from $\left\|\boldsymbol{\psi}_{\mathrm{cs},k}(t)\right\|_2^2 \geq \left\|\boldsymbol{\omega}_{\mathrm{cs},k}(t)\right\|_2^2$ according to (35c) and (37). Since the impulse response to the unit-impulse $\mathbf{w}(t) = \mathbf{e}_k\delta(t)$ is equivalent to the initial state response under the initial condition $\mathbf{X}_k(0) = \mathcal{B}_{\mathbf{w},\mathrm{c}}\mathbf{e}_k$, the upper bound of the $\mathcal{H}_2$ cost function (31) is

$$\begin{aligned} \sum_{k=0}^{n_w}\int_0^\infty \|\mathbf{Z}_k(t)\|^2\,dt &< \sum_{k=0}^{n_w} V(\mathbf{X}_k(0)) \\ &= \sum_{k=0}^{n_w}(\mathcal{B}_{\mathbf{w},\mathrm{cs}}\mathbf{e}_k)^\top\mathbf{P}_{\mathrm{cs}}\mathcal{B}_{\mathbf{w},\mathrm{cs}}\mathbf{e}_k \\ &= \mathrm{trace}\{\mathcal{B}_{\mathbf{w},\mathrm{cs}}^\top\mathbf{P}_s\mathcal{B}_{\mathbf{w},\mathrm{cs}}\}. \quad \square \end{aligned}$$

Appendix C. Proof of Theorem 2

For internal stability analysis, the additive noise $\mathbf{w}(t)$ is set to zero. According to Theorem 1, the solution to (39) stabilizes the PCE-transformed closed-loop system (28), thus we have $\mathbf{X}(\infty) = \mathbf{0}$. This implies that the PCE-transformed approximated state $\hat{\mathbf{x}}(t,\boldsymbol{\xi}) = \Phi_{\mathbf{x}}^\top(\boldsymbol{\xi})\mathbf{X}(t)$ goes to zero as time goes to infinity. To show the internal mean square stability of the original system (1) under the synthesized SOF control, the PCE truncation error $\tilde{\mathbf{x}}(t,\boldsymbol{\xi})$ needs to be discussed in the following.

For any normalized orthogonal PCE bases, the first basis function $\phi_0(\boldsymbol{\xi})$ in (12) is equal to 1 (Xiu, 2010). Therefore, using the definition of $\Phi_{\mathbf{s}}(\boldsymbol{\xi})$ in (13), (34) implies

$$\begin{aligned} \mathbb{E}_{\boldsymbol{\xi}}\{\|\mathbf{r}_{\mathbf{s}}(t,\boldsymbol{\xi})\|_2^2\} &\leq \sum_{i=0}^{N_p}\mathbb{E}_{\boldsymbol{\xi}}\left\{\phi_i^2(\boldsymbol{\xi})\,\|\mathbf{r}_{\mathbf{s}}(t,\boldsymbol{\xi})\|_2^2\right\} \\ &= \mathbb{E}_{\boldsymbol{\xi}}\left\{\|\Phi_{\mathbf{s}}(\boldsymbol{\xi})\mathbf{r}_{\mathbf{s}}(t,\boldsymbol{\xi})\|_2^2\right\} \leq \rho_{\mathbf{s}}^2\,\|\mathbf{X}(t)\|_2^2. \end{aligned} \tag{C.1}$$

As such, combining (25), (A.5) and (C.1) gives

$$\mathbb{E}_{\boldsymbol{\xi}}\{\left\|\mathbf{A}_{\mathrm{cl}}(\boldsymbol{\xi})\tilde{\mathbf{x}}(\infty,\boldsymbol{\xi})\right\|_2^2\} = \mathbf{0},\ \mathbb{E}_{\boldsymbol{\xi}}\{\left\|\mathbf{C}(\boldsymbol{\xi})\tilde{\mathbf{x}}(\infty,\boldsymbol{\xi})\right\|_2^2\} = \mathbf{0},$$

which can be further expressed as

$$\mathbb{E}_{\boldsymbol{\xi}}\left\{\left\|\begin{bmatrix}\mathbf{A}_{\mathrm{cl}}(\boldsymbol{\xi})\\ \mathbf{C}(\boldsymbol{\xi})\end{bmatrix}\tilde{\mathbf{x}}(\infty,\boldsymbol{\xi})\right\|_2^2\right\} = \mathbf{0}. \tag{C.2}$$

Since the detectability of $(\mathbf{A}(\boldsymbol{\xi}), \mathbf{C}(\boldsymbol{\xi}))$ for any $\boldsymbol{\xi} \in \Xi$ implies that $\begin{bmatrix}\mathbf{A}^\top(\boldsymbol{\xi}) & \mathbf{C}^\top(\boldsymbol{\xi})\end{bmatrix}^\top$ has full column rank (see Theorem 3.4 in Zhou et al., 1996), the matrix

$$\begin{bmatrix}\mathbf{A}_{\mathrm{cl}}(\boldsymbol{\xi})\\ \mathbf{C}(\boldsymbol{\xi})\end{bmatrix} = \begin{bmatrix}\mathbf{I} & \mathbf{B}(\boldsymbol{\xi})\mathbf{K}\\ \mathbf{0} & \mathbf{I}\end{bmatrix}\begin{bmatrix}\mathbf{A}(\boldsymbol{\xi})\\ \mathbf{C}(\boldsymbol{\xi})\end{bmatrix}$$

is also of full column rank for any $\boldsymbol{\xi} \in \Xi$. Consequently, (C.2) leads to

$$\mathbb{E}_{\boldsymbol{\xi}}\left\{\left\|\tilde{\mathbf{x}}(\infty,\boldsymbol{\xi})\right\|_2^2\right\} = \mathbf{0},$$

which further implies

$$\begin{aligned} \mathbb{E}_{\boldsymbol{\xi}}\left\{\|\mathbf{x}(\infty,\boldsymbol{\xi})\|_2^2\right\} &= \mathbb{E}_{\boldsymbol{\xi}}\left\{\left\|\Phi_{\mathbf{x}}^\top(\boldsymbol{\xi})\mathbf{X}(\infty) + \tilde{\mathbf{x}}(\infty,\boldsymbol{\xi})\right\|_2^2\right\} \\ &= \mathbb{E}_{\boldsymbol{\xi}}\left\{\left\|\tilde{\mathbf{x}}(\infty,\boldsymbol{\xi})\right\|_2^2\right\} = \mathbf{0} \end{aligned}$$

due to $\mathbf{X}(\infty) = 0$.

All the above analysis shows that under the condition specified in Theorem 2, the stability of the PCE-transformed closed-loop system (28) indeed ensures $\mathbb{E}_{\boldsymbol{\xi}}\left\{\|\mathbf{x}(\infty,\boldsymbol{\xi})\|_2^2\right\} = \mathbf{0}$, i.e., the internal mean square stability of the original system (1) under control.

References

Ahn, C. K., Shi, P., & Li, H. (2018). *H_2 output-feedback control with finite multiple measurement information*. *IEEE Transactions on Automatic Control*, *63*(8), 2588–2595.

Bergner, L., & Kirches, C. (2018). The polynomial chaos approach for reachable set propagation with application to chance-constrained nonlinear optimal control under parametric uncertainties. *Optimal Control Applications & Methods*, *39*(2), 471–488.

Bhattacharya, R. (2019). Robust LQR design for systems with probabilistic uncertainty. *International Journal of Robust and Nonlinear Control*, *29*(10), 3217–3237.

Boyarski, S., & Shaked, U. (2005). Robust $\mathcal{H}_\infty$ control design for best mean performance over an uncertain-parameters box. *Systems & Control Letters*, *54*(6), 585–595.

Brewer, J. (1978). Kronecker products and matrix calculus in system theory. *IEEE Transactions on Automatic Control*, *25*(9), 772–781.

Chang, X., Park, J. H., & Zhou, J. (2015). Robust static output feedback $\mathcal{H}_\infty$ control design for linear systems with polytopic uncertainties. *Systems & Control Letters*, *85*, 23–32.

Dai, L., Xia, Y., & Gao, Y. (2015). Distributed model predictive control of linear systems with stochastic parametric uncertainties and coupled probabilistic constraints. *SIAM Journal on Control and Optimization*, *53*(6), 3411–3431.

Dong, J., & Yang, G. H. (2013). Robust static output feedback control synthesis for linear continuous systems with polytopic uncertainties. *Automatica*, *49*(6), 1821–1829.

Fisher, J., & Bhattacharya, R. (2009). Linear quadratic regulation of systems with stochastic parameter uncertainties. *Automatica*, *45*(12), 2831–2841.

Fletcher, L. R. (1981). Output feedback matrices in the presence of direct feedthrough. *International Journal of Systems Science*, *12*(12), 1493–1495.

Geromel, J. C., Korogui, R. H., & Bernussou, J. (2007). $\mathcal{H}_2$ and $\mathcal{H}_\infty$ robust output feedback control for continuous time polytopic systems. *IET Control Theory & Applications*, *1*(5), 1541–1549.

Goh, K. C., Safonov, M. G., & Papavassilopoulos, G. P. (1994). A global optimization approach for the BMI problem. In *Proceedings of 33rd IEEE Conference on Decision and Control* (pp. 2009–2014).

Hosoe, Y., Hagiwara, T., & Peaucelle, D. (2018). Robust stability analysis and state feedback synthesis for discrete-time systems characterized by random polytopes. *IEEE Transactions on Automatic Control*, *63*(2), 556–562.

Hover, F. S., & Triantafyllou, M. S. (2006). Application of polynomial chaos in stability and control. *Automatica*, *42*(5), 789–795.

Hsu, S. C., & Bhattacharya, R. (2017). Design of stochastic collocation based linear parameter varying quadratic regulator. In *Proceedings of American Control Conference* (pp. 2375–2380).

Kim, K. K. K., Shen, D. E., Nagy, Z. K., & Braatz, R. D. (2013). Wiener's polynomial chaos for the analysis and control of nonlinear dynamical systems with probabilistic uncertainties. *IEEE Control Systems*, *33*(5), 58–67.

Konda, U., Singla, P., Singh, T., & Scott, P. D. (2011). State uncertainty propagation in the presence of parametric uncertainty and additive white noise. *Journal of Dynamic Systems, Measurement, and Control*, *133*(5), Article 051009.

Kočvara, M., & Stingl, M. (2012). PENNON: Software for linear and nonlinear matrix inequalities. In M. F. Anjos, & J. B. Lasserre (Eds.), *Handbook on Semidefinite, Conic and Polynomial Optimization* (pp. 755–791). New York: Springer.

Lee, D. H., Joo, Y. H., & Tak, M. H. (2015). Periodically time-varying memory static output feedback control design for discrete-time LTI systems. *Automatica*, *52*, 47–54.

Lefebvre, T., De Belie, F., & Crevecoeur, G. (2020). A framework for robust quadratic optimal control with parametric dynamic model uncertainty using polynomial chaos. *Optimal Control Applications & Methods*, *41*(3), 833–848.

Li, H., & Zhang, D. (2007). Probabilistic collocation method for flow in porous media: Comparisons with other stochastic methods. *Water Resources Research*, *43*(9), W09409.

Luchtenburg, D. M., Brunton, S. L., & Rowley, C. W. (2014). Long-time uncertainty propagation using generalized polynomial chaos and flow map composition. *Journal of Computational Physics*, *274*, 783–802.

Lucia, S., Paulson, J. A., Findeisen, R., & Braatz, R. D. (2017). On stability of stochastic linear systems via polynomial chaos expansions. In *Proceedings of American Control Conference* (pp. 5089–5094).

Nandi, S., & Singh, T. (2018). Chance-constraint-based design of open-loop controllers for linear uncertain systems. *IEEE-ASME Transactions on Mechatronics*, *23*(4), 1952–1963.

Paulson, J. A., Harinath, E., Foguth, L. C., & Braatz, R. D. (2015). Nonlinear model predictive control of systems with probabilistic time-invariant uncertainties. In *Proceedings of 5th IFAC Conference on Nonlinear Model Predictive Control* (pp. 16–25).

Paulson, J. A., & Mesbah, A. (2019). An efficient method for stochastic optimal control with joint chance constraints for nonlinear systems. *International Journal of Robust and Nonlinear Control*, *29*(15), 5017–5037.

Petersen, I. R., & Tempo, R. (2014). Robust control of uncertain systems: Classical results and recent developments. *Automatica*, *50*(5), 1315–1335.

Piga, D., & Benavoli, A. (2017). A unified framework for deterministic and probabilistic D-stability analysis of uncertain polynomial matrices. *IEEE Transactions on Automatic Control*, *62*(10), 5437–5444.

Rosa, T. E., Morais, C. F., & Oliveira, R. C. (2018). New robust LMI synthesis conditions for mixed gain-scheduled reduced-order DOF control of discrete-time LPV systems. *International Journal of Robust and Nonlinear Control*, *28*(18), 6122–6145.

Rosenblatt, M. (1952). Remarks on a multivariate transformation. *The Annals of Mathematical Statistics*, *23*(3), 470–472.

Sadabadi, M. S., & Peaucelle, D. (2016). From static output feedback to structured robust static output feedback: A survey. *Annual Reviews in Control*, *42*, 11–26.

Salavati, S., Grigoriadis, K., & Franchek, M. (2019). Reciprocal convex approach to output-feedback control of uncertain LPV systems with fast-varying input delay. *International Journal of Robust and Nonlinear Control*, *29*(16), 5744–5764.

Scherer, C., Gahinet, P., & Chilali, M. (1997). Multiobjective output-feedback control via LMI optimization. *IEEE Transactions on Automatic Control*, *42*(7), 896–911.

Shen, D., Lucia, S., Wan, Y., Findeisen, R., & Braatz, R. D. (2017). Polynomial chaos-based $\mathcal{H}_2$-optimal static output feedback control of systems with probabilistic parameter uncertainties. In *Proceedings of 20th IFAC World Congress* (pp. 3595–3600).

Skelton, R. E., Iwasaki, T., & Grigoriadis, K. M. (1997). *A Unified Algebraic Approach to Control Design*. London: Taylor & Francis.

Tempo, R., Calafiore, G., & Dabbene, F. (2013). *Randomized Algorithms for Analysis and Control of Uncertain Systems* (2nd ed.). London: Springer-Verlag.

VanAntwerp, J., & Braatz, R. D. (2000). A tutorial on linear and bilinear matrix inequalities. *Journal of Process Control*, *10*(4), 363–385.

Xiu, D. (2010). *Numerical Methods for Stochastic Computations: A Spectral Method Approach*. New Jersey: Princeton University Press.

Xiu, D., & Karniadakis, G. E. (2002). The Wiener–Askey polynomial chaos for stochastic differential equations. *SIAM Journal on Scientific Computing*, *24*(2), 619–644.

Yin, Y., Liu, Y., Teo, K. L., & Wang, S. (2018). Event-triggered probabilistic robust control of linear systems with input constrains: By scenario optimization approach. *International Journal of Robust and Nonlinear Control*, *28*(1), 144–153.

Zhou, K., Doyle, J. C., & Glover, K. (1996). *Robust and Optimal Control*. New Jersey: Prentice-Hall.

Yiming Wan received a Ph.D. in Automatic Control from Tsinghua University in 2013. From 2013 to 2016, he was a postdoctoral researcher at Delft Center for Systems and Control, Delft University of Technology, The Netherlands. During 2016 to 2018, he was a Research Associate at the Massachusetts Institute of Technology, United States. Since February 2018, he has been an Associate Professor in the School of Artificial Intelligence and Automation, Huazhong University of Science and Technology, Wuhan, China. His research interests include fault-tolerant control, industrial data analytics, state and parameter estimation, and model predictive control.

Dongying Erin Shen is a Data Scientist at Amgen in Cambridge, Massachusetts. Past professional positions include as a Senior Engineer at Amgen from 2019 to 2021 and as the Process Control Engineer and PAT Lead for Continuus Pharmaceuticals, Inc. from 2017 to 2019. She received a B.S. from the California Institute of Technology and an M.S. and Ph.D. in 2016 and 2018 from the Massachusetts Institute of Technology. Her interests are in first-principles modeling, process data analytics, machine learning, and optimal control and their applications to pharmaceutical manufacturing.

Sergio Lucia received an M.Sc. in electrical engineering from the University of Zaragoza, Spain, and the Dr. Ing. in optimization and automatic control from the Technische Universität Dortmund, Germany. He joined the Otto-von-Guericke Universität Magdeburg and visited the Massachusetts Institute of Technology as a Postdoctoral Fellow. In 2017, he was appointed Assistant Professor at the Technische Universität Berlin, Germany. Since October 2020, he is a Professor and Head of the Laboratory of Process Automation Systems at the Technische Universität Dortmund, Germany. His research interests include decision-making under uncertainty, distributed control, and the interplay between machine learning techniques and control theory.

Rolf Findeisen received an M.S. from the University of Wisconsin–Madison and a Ph.D. from the University of Stuttgart. He was a Research Assistant with the Automatic Control Laboratory, ETH Zürich and a Researcher with the Institute for Systems Theory and Automatic Control, University of Stuttgart. He heads the Systems Theory and Automatic Control Laboratory, Otto-von-Guericke University Magdeburg, where he is a full chaired Professor. He was the IPC Co-Chair of the 2020 IFAC World Congress and is an IFAC TC Chair and IEEE CSS TC Vice-Chair. Research interests include learning-based control, predictive control theory, autonomous systems, and cyber–physical systems.

Richard D. Braatz is the Edwin R. Gilliland Professor at the Massachusetts Institute of Technology (MIT) where he does research in control theory and its applications to advanced manufacturing. He received an M.S. and Ph.D. from the California Institute of Technology and was a Professor at the University of Illinois at Urbana-Champaign and a Visiting Scholar at Harvard University before moving to MIT. Recognitions include the AACC Donald P. Eckman Award and the IEEE CSS Antonio Ruberti Young Researcher Prize. He is a Fellow of IEEE and IFAC and a member of the U.S. National Academy of Engineering.